Contents lists available at ScienceDirect

Food Hydrocolloids

Construction of 3D printed reduced-fat meat analogue by emulsion gels. Part I: Flow behavior, thixotropic feature, and network structure of soy protein-based inks

Mahdiyar Shahbazi [a,*], Henry Jäger [a,*], Rammile Ettelaie [b], Jianshe Chen [c]

[a] Institute of Food Technology, University of Natural Resources and Life Sciences (BOKU), Muthgasse 18, 1190, Vienna, Austria
[b] Food Colloids and Bioprocessing Group, School of Food Science and Nutrition, University of Leeds, Leeds, LS2 9JT, UK
[c] Food Oral Processing Laboratory, School of Food Science & Biotechnology, Zhejiang Gongshang University, Hangzhou, China

A B S T R A C T

The fabrication of high-quality low-fat 3D printed foods is strongly dependent on the development of shear-thinning, viscoelastic, and thixotropic ink with a monomodal particle size distribution. In this study, oil was partially or totally replaced with hydrophobically modified biosurfactants (acetylated starch, octenyl succinic anhydride starch, ethyl (hydroxyethyl) cellulose, and dodecenyl succinylated inulin) in a soy protein-based emulsion to produce the desired reduced-fat emulsion gels for potential applications in the 3D printing process. These reduced-fat emulsion gels exhibited *pseudoplastic* behavior with viscoelastic properties, where viscosity recovery, frequency crossover point, and storage modulus were found to increase with increasing biosurfactants ratio. Higher levels of surface-active biopolymers also yielded inks with lower creep compliance, a smaller droplet size having a more uniform distribution, and possessing improved structural strength and storage stability. Spherical droplets of inks with higher ratios of biosurfactants remained well dispersed. The differences in molecular weight and radius of gyration of biosurfactants accounted for the observed differences in flow behavior and emulsion stability, where inks including dodecenyl succinylated inulin and ethyl (hydroxyethyl) cellulose offered stable structures with strong gel-like properties compared to acetylated and octenyl succinic anhydride starches. All ink networks were also dynamic and recoverable, thus demonstrating the potential of these reduced-fat inks in 3D printing processes.

1. Introduction

In recent years there is an increased demand for protein-rich ingredients derived from non-animal sources, as possible alternatives to animal-sourced proteins in meat products. Factors influencing this trend include the growth of world populations and restricted natural resources, resulting in the utilization of less expensive and more sustainable plant-based proteins (Malav, Talukder, Gokulakrishnan, & Chand, 2015). Soy protein, as an important source of essential and non-essential amino acids, shows good physicochemical and functional properties and has widely been used as a plant source in food formulations (Malav et al., 2015; Bohrer, 2019; Wang et al., 2020). It is a promising resource to serve in the preparation of meat alternatives on the account of providing a gel-like structure. However, soy protein alone cannot provide the well-defined layered and fibrous structure of traditional meats (Asgar, Fazilah, Huda, Bhat, & Karim, 2010). It is stated that the application of biopolymeric surfactants in the 3D printing technology, one may efficiently improve the textural features of meat analogues (Zhang, Pandya, McClements, Lu, & Kinchla, 2021). The structural network developed by this multisystem offers the required consistency needed in meat analogues, potentially achieving the fibrous-like texture of the resultant meat products.

There has been also a heightened demand for healthy meat analogue products developed with reduced fat and cholesterol content. In the meat analogue products, one promising approach to reducing fat content involves the addition of various specific biopolymers as substitute fat replacers, which can include active ingredients that may provide further health benefits (Malav et al., 2015; Bohrer, 2019). This aspect is

particularly important for the meat industry, as some meat analogues comprise high-fat levels, which can vary anywhere from 0 to 20% (Asgar et al., 2010; Bohrer, 2019). As fat is not just a simple caloric filler hidden in a protein matrix, a fat-replacement strategy for processed meats must thus address the diverse influence of fat on structure, texture, and mouthfeel. Using the approach of fat substitution, it is possible to attain satisfactory textural and sensory features, since the fat replacers can form a biopolymeric gel network in the presence of water, and therefore change the product texture and offer a fat-like mouthfeel.

Biopolymeric surfactants are important for a variety of industrial applications due to their low cost, biodegradability, biocompatibility, improved flow behavior, and surface-active features. The emulsion stability of tuned cellulosic compounds continues to receive distinct attention because of the industrial significance of this type of surface-active biopolymer. It is shown that ethyl (hydroxyethyl) cellulose (EHEC) can stabilize O/W emulsions through an associative thickening mechanism, thus improving the rheological properties of the continuous phase (Karlberg, Thuresson, & Lindman, 2005). Octenyl succinic anhydride (OSA) starch is another surface-active biopolymer because of attaching hydrophobic octenyl-succinate groups to the hydrophilic backbone. Owing to the free hydroxyl groups in starch molecules, as well as the carboxylic groups linked to the octenyl-succinate chain, OSA starch is widely utilized as an emulsifying agent in the food industry to efficiently stabilize emulsions for long storage time (Ding et al., 2021). Acetylated starch as a biopolymeric surfactant can form a very densely packed interface layer on the surface of spherical oil droplets. The inclusion of an acetyl group in starch backbones allows better emulsification properties and higher resistance to phase separation. The physically stable O/W can also be effectively developed through hydrophobically modified inulin as a biosurfactant, even when subjected to shear force, high temperature, salt, and low pH conditions (Kiumarsi, Majchrzak, Yeganehzad, Jäger, & Shahbazi, 2020). It is applied commercially as an alternative to common surfactants employed in colloidal systems to stabilize the solid/droplet particles dispersed in a liquid phase (Tadros, Vandamme, Booten, Levecke, & Stevens, 2004).

The introduction of 3D printing to food science has created the opportunity for major innovations in the food industry towards the development of modern foods (Shahbazi & Jäger, 2020). To establish the 3D printing process as an effective device to construct 3D food structures, a thorough understanding of the utilized components and process approaches to improve printing performance is necessary. In this sense, the rheological properties of printable ink can directly impact the printing performance and shape fidelity of the printed constructs. Generally, a printable biopolymeric ink must offer a well-defined shear-thinning behavior, have viscoelastic character, and displays thixotropic properties to allow the correct extrusion out through a nozzle tip. The flow behavior of 3D printed inks is commonly assigned to be the quality indicator of the end-products and offers essential information for printing processes, and therefore determines the suitability of the components to enhance the functionality of the final 3D objects being printed. The biggest challenge for 3D food printing, then, remains to realize the right kind of texture to deliver the finest resolution of printed constructs with an appreciable mouthfeel. Pure proteins lack the stability needed to form a 3D structure, so they have to be combined with other biopolymers (Godoi, Prakash, & Bhandari, 2016). A precise and accurate 3D structure might not be successfully printed without adding other suitable biopolymers for controlling the flow and rheological behavior, enhancing mechanical properties, and improving the microstructure through the gelation and aggregation of such macromolecules (Shahbazi & Jäger, 2020).

The modified supramolecular biopolymers can be used in the 3D printing to provide constructs with custom-designed structures, personalized nutrition, and an improved printing process. In this regard, surface-active biopolymers offer supramolecular functional properties to the printable ink dispersion, which can adjust its flow behavior and reinforce the mechanical strength of 3D printed architectures.

Therefore, a systematic study to explore the possibility of developing reduced-fat emulsion gels with surface-active biopolymers presents innovative prospects to fabricate a well-defined printable ink possessing the required shear-thinning, viscoelastic, and thixotropic properties to avoid various complication that can arise during the printing process.

In view of the above, the main objective of the current work was to study the development of a reduced-fat emulsion gel based on soy protein for potential application in the 3D printing process, with consideration of the functionality of different amphiphilic surface-active biopolymer variants.

2. Methods and materials

2.1. Material

The soy protein isolate (SPI) (moisture: 4.83%, fat: 0.32%, protein: 92.88%, ash: 3.40%, pH: 7.09, and viscosity of 1% wt. solution: 10.0 cP) was obtained from Archer Daniels Midland Company (ADM, Decatur, IL). Inulin was obtained from FXL (Cosucra Warcoing, Belgium). The FXL refers to the long-chain inulin with a polymerization degree value of ≥23. Then, it was modified by (2-dodecen-1-yl)succinic anhydride (Kiumarsi et al., 2019). The ethyl (hydroxyethyl) cellulose (EHEC) was obtained from Akzo Nobel Surface Chemistry AB (Stenungsund, Sweden). According to the manufacturer, the EHEC had an ethyl substitution degree of ≈0.8 and a molar degree of hydroxyethyl substitution of ≈2.1. Acetylated starch (DM-239), a modified food starch derived from wheat with 6.8% moisture content, < 0.7% fat, <1% ash, and amylose/amylopectin ratio of 23:77 (AACC, 2000; Morrison & Laignelet, 1983) and degree substitution of 1.8 (Elomaa et al., 2004), was supplied by Dongguan Dongmei Food Co., Ltd (Guangdong, China). OSA starch was obtained from National Starch Food Innovation (Hamburg, Germany). Dimethyl sulfoxide (DMSO) was purchased from Sigma-Aldrich (Steinheim, Germany). Canola oil and salt were obtained from the local market. Beet juice extract was purchased from Nature's Bounty (Winnipeg, Manitoba, Canada).

2.2. Capillary viscometer

Coil-overlap concentration ($c*$), intrinsic viscosity (η), and coil-overlap parameters c [η] of each biosurfactant were determined by Cannon-Ubbelohde capillary viscometer (9721-K56, size 75, Cannon Instruments Co., Germany), with $k = 0.007690$ mm^2 s^{-2}, coupled with a thermostatic water bath under defined temperature control (25 ± 1 °C). Different amounts of the biosurfactants (0.2–5.0 g L^{-1}) were dissolved in DMSO to cover the span of concentrations from dilute to the semi-dilute areas. The solvent was obtained by introducing 9 L of DMSO to 1 L of deionized water (90% v/v) and stirred at 60 °C for 30 min to obtain a homogeneous solution. Starting with, precisely 2 mL of each solution, the system was manually diluted upon developing at least three efflux time readings at each concentration (Shahbazi et al., 2017). Then, the relative viscosity (η_{rel}), reduced viscosity (η_{red}), and inherent viscosity (η_{inh}) were calculated by Eqs. (1)–(3), respectively, as follows:

$$\eta_{rel} = \frac{\eta}{\eta_0} = \frac{t}{t_0} \cdot \frac{\rho}{\rho_0} \tag{1}$$

$$\eta_{red} = \frac{(\eta_{rel} - 1)}{c} \tag{2}$$

$$\eta_{inh} = \frac{\ln (\eta_{rel})}{c} \tag{3}$$

Here, t/t_o and ρ/ρ_o are the ratio of efflux time of solution to solvent and the proportion of the density of the solution to the solvent, respectively. The (η_{rel}-1) is specific viscosity (η_{sp}) and the concentration of the biopolymers is represented as c.

The intrinsic viscosity is obtained from the extrapolation of Ln (η_{rel})/

c and η_{sp}/c to infinite dilution according to Huggins's equation (4) and Kraemer's equation (5) as follows (Huggins, 1942; Kraemer, 1938):

$$\frac{\eta_{sp}}{c} = [\eta] + K_1[\eta]^2 c \qquad (4)$$

$$\frac{Ln(\eta_{rel})}{c} = [\eta] + K_2[\eta]^2 c \qquad (5)$$

where, K_1 and K_2 are the Huggins's and the Kraemer's constants, respectively (Morris, Cutler, Ross-Murphy, Rees, & Price, 1981).

2.3. Macromolecular characteristics by SEC-MALLS

Macromolecular properties including molecular weight, polydispersity index, and radius of gyration of each biosurfactant were evaluated by size exclusion chromatography (SEC) equipped with a multiangle laser light scattering (MALLS) photometer (DAWN EOS, Wyatt Technology Co., Santa Barbara, CA) through a refractive index of 1.33. An Ultrahydrogel™ column (7.8 mm × 300 mm, Waters Co., Milford, MA) was employed as the SEC apparatus. An Optilab refractometer (Dawn, Wyatt Technology Co., Santa Barbara, CA) was also simultaneously connected. The injection volume was 75 mL and a flow rate of 1.5 mL min^{-1} was considered for all experiments. The refractive index increment (*dn/dc*) value of the samples was obtained through the Optilab refractometer (λ = 690 nm) at 25 °C with a value of 0.140 mL g^{-1}.

2.4. Preparation of SPI-based inks

Three batches (1 L each) of SPI-based ink emulsion were developed with a similar method using the following formulation. The SPI aqueous dispersion was obtained through dispersing SPI powder (40 g) into part of the deionized water, with the rest of the water being used to disperse the biosurfactant variants. Subsequently, salt (0.1 g) and beet juice extract as a colorant (0.3% v/v) were added to the SPI-based dispersion. Then, the protein-based dispersion was gently stirred at 35 °C for 120 min using a magnetic heater-stirrer. Simultaneously, 10% (v/v) canola oil was added to the SPI-based dispersion through a burette. The obtained emulsions were mixed manually and stirred with an Ultra-Turrax at speed of 5000 rpm for 5 min. Separately, each biosurfactant was dispersed into deionized water with a concentration of 4 g/100 g (biosurfactant/water) and stirred at 50 °C for 120 min (see Fig. A.1 in Supplementary Materials).

To produce the reduced-fat emulsion gels, the biosurfactant dispersions were individually incorporated into the SPI-based emulsion to substitute 20, 40, 60, 80, and 100% of the oil in the emulsion system, and heated at 35 °C with continuous stirring for 120 min. In this sense, canola oil was partially or totally replaced by each biosurfactant solution (100:0%, 80:20%, 60:40%, 40:60%, 20:80%, and 0:100%). The obtained SPI-based emulsion gels were then subsequently homogenized at room temperature using an M110-PS Microfluidizer processor (Microfluidics international Corp., Newton, MA) at 5 MPa for two cycles. The SPI-based inks prepared with EHEC, OSA starch, acetylated starch, and dodecenyl succinylated (DS) inulin were named as MAC, MAO, MAA, and MAI, respectively, and the respected ratios of biosurfactant to oil were included in the abbreviation (for example, MAC-20, MAC-40, MAC-60, MAC-80, and MAC-100). All printable inks were conditioned in a controlled bio-chamber (ACS Sunrise 700 V, Alava Ingenieros, Madrid, Spain) at 25 °C with a relative humidity of (45 ± 2)% for 48 h before experiments. Before the process, sodium azide (0.005 g L^{-1}) was added to the emulsion gels to prevent bacterial growth. The pH of these inks was between 5.20 and 5.60, which was close to the pH of the meat (Watanabe, Daly, & Devine, 1996).

2.5. Rheological measurement of inks

2.5.1. Steady rheological properties

Flow properties of printable ink emulsions as influenced by biosurfactant types and levels were investigated by rheometer (AR 2000; TA Instruments, New Castle, DE). The experiments were carried out at 25 °C using parallel plate geometry with a 40 mm diameter. Shear stress (τ) values were obtained as a function of increasing shear rate from 0.1–1000 s^{-1}. The stress-strain curves were obtained by plotting the recorded shear stress against the applied shear rate. The best equation was designated through statistical analysis and rheological variables were determined from the model fit. Accordingly, the consistency index, flow behavior index, and yield stress values were calculated by fitting the Herschel-Bulkley model (Eq. (6)) to the data. The efficiency of the Herschel-Bulkley model was proved by residual plots and normally test via statistical software of Graph Pad In Stat (version 3.06, Graph Pad Inc., San Diego, CA):

$$\tau = \tau_0 + K\dot{\gamma}^n \qquad (6)$$

In the above equation, τ_0 is the yield stress, K is the consistency index, $\dot{\gamma}$ is the shear rate (s^{-1}), and n is the flow behavior index. The diagnostic analysis of the Herschel-Bulkley model exposed the residual plots with no systematic patterns and normally distributed with $P > 0.1$ for all printable inks offering a Gaussian distribution ($R^2 \approx 1$) (Shahbazi, Jäger, & Ettelaie, 2021a).

2.5.2. Dynamic rheological characterization

Dynamic rheological measurements of printable inks were carried out using an AR-G2 rheometer (TA Instruments, West Sussex, UK) coupled with a heating circulator (Julabo, F-12, Seelbach, Germany) at 25 °C. A cone and plate geometry (60 mm diameter, 2° cone angle, and 58 µm gap) was utilized for the experiment. A strain sweep test was conducted (0.01–100%, 1.0 Hz) to determine the limit of the linear viscoelastic region (LVR). Furthermore, the frequency sweep test (0.1–100 Hz) of inks was carried out in the LVR. The critical strain for the inks was calculated to be the strain at which the storage modulus (G') deviated by more than 5% from the prior magnitude (data not shown). Then, the frequency sweep evaluations were performed at 50% of the smallest critical strain determined (1.0%) to ensure the tests were carried out within the LVR. The rheological parameters including G', loss modulus (G''), strain crossover pint (γ_c), and frequency crossover point (ω_c) were obtained from the manufacturer supplied computer software (TRIOS, TA Instruments, West Sussex, UK) (Shahbazi, Jäger, Ahmadi, & Lacroix, 2020).

2.6. Creep and creep-recovery test

The creep is considered as the slow progress of relaxation of strains at a practical constant applied shear stress (τ_0). The creep-recovery experiment was carried out to obtain the compliance extent in creep and recovery phases. In this case, the stress sweep (1 Hz, 0.1–100 Pa) was performed to determine oscillatory yield value, and then τ_0 values used for ink variants were considered as around 50% of the yield value (Fig. A.2 in Supplementary Material). The ink samples were placed in parallel-plate flow chambers (diameter 40 mm, gap 1 mm) at a temperature of 25 °C. The creep experiment involved the utilization of a rapidly applied constant shear stress inside the LVR area, from 0 to 600 s, while monitoring the sample strain at regular time intervals. Regarding the recovery phase, the applied stress was rapidly removed ($\tau_{applied}$ = 0.0 Pa) and then the ink recovery was recorded by measuring the strain for a further period of 600 s, at an identical temperature to that in the creep phase. The recovery value was evaluated immediately upon the completion of the creep phase. The time interval was found to be appropriate for the ink variants to attain steady strain extents. The calculated strain and recovery could be taken as creep compliance and

creep-recovery compliance (*J*) (Eq. (7)). This causes a material-dependent outcome, independent of the value of employed shear stress (Shahbazi et al., 2021a). The creep-recovery percentages of inks were then calculated based on Eq. (8).

$$J(t) = \gamma(t) / \tau_0 \qquad (7)$$

$$\text{Percentage recovery} = (J_m - J_e) / J_m \times 100\% \qquad (8)$$

Here, *J(t)* (Pa^{-1}) is creep compliance, γ is the measured strain, *t* is time, τ_0 is the constant applied shear stress, J_m (Pa^{-1}) is the maximum creep, J_e (Pa^{-1}) is the equilibrium creep compliance after recovery.

2.7. Three interval thixotropy test (3-ITT)

The 3-ITT experiment was conducted to evaluate the time-dependent nature of the printable inks and recovering capacities of their initial structures upon application of low-shear rate after high-shear condition. The 3-ITT involved a three-step shear rate test, where the first one contained a constant shear rate to detect the ink reference phase without interrupting the microstructure. This involved applying a constant shear rate of 1 s^{-1} for 250 s. This was followed by the second interval, in which a constant shear rate of 80 s^{-1} for 100 s was applied to disrupt the microstructure of the sample. The third interval included a similar experiment like that in the first interval, determining the reversible reformation of the microstructure (degree and speed of recovery) of printable ink.

2.8. Droplet size

The droplet size distributions of printable ink emulsions were obtained immediately after emulsion preparation and further experiments were conducted periodically for up to 21 days through a Malvern Mastersizer (MS 2000, Malvern Instruments Ltd., Worcestershire, UK) at room temperature (25 °C). Approximately 1 mL of each ink-based emulsion was diluted to 500 mL of water and the pump rate in the dispersion part was set at 1800 rpm (Hydro 2000MU, Malvern Instruments, Worcestershire, UK). The refractive indices of canola oil and water were set at 1.433 and 1.323, respectively, and the adsorption index was adjusted to 0.001. The average droplet size was characterized in terms of the surface area mean diameter (*d $_{3,2}$*) and volume mean diameter (*d $_{4,3}$*) to detect the specific surface area of freshly prepared emulsions and changes in droplet size over time, respectively (Kokubun, Ratcliffe, & Williams, 2015).

2.9. Confocal laser scanning microscopy (CLSM)

The SPI-based ink microstructure was imaged through CLSM at 20 °C after emulsion preparation. Exactly, 5 mL of inks were stained with a suitable extent of Nile Blue A (1.0%, w/v) in distilled water, or the mixture of Nile Blue A (1%, w/v) and Nile Red (0.1%, w/v) in 1,2-propanediol (containing distilled water, 20 μL g^{-1}) to mark the protein and/or biosurfactants and oil droplet, respectively. The concentration of both Nile blue A and Nile red solution was 0.01% (w/v) (Auty, Twomey, Guinee, & Mulvihill, 2001). The excitation wavelength of fluorescent in the ink was 488 nm (Nile red) and 633 nm (Nile blue A). The interfacial network structure was imaged immediately after staining by an FV-300 confocal scanning unit (Olympus, Tokyo, Japan) equipped with an Olympus IX71 inverted microscope and an argon-ion laser. All images were taken at 40 × magnification (oil immersion, numeric aperture 1.30) and processed using the Olympus Fluoview software (Shahbazi, Jäger, & Ettelaie, 2021b).

2.10. Statistical analysis

All experiments were performed in triplicates and the mean and standard deviation of the data were reported. Analysis of variance (ANOVA) was applied for the determination of the main impacts of the examined independent factors, and their interactions on the instrumental data. Duncan's multiple range test was utilized to separate means of data once significant differences (*P* < 0.05) were observed.

3. Results and discussion

3.1. Coil-overlap point, intrinsic viscosity, and coil-overlap parameter of biosurfactants

A complete treatment of the viscosity for surface-active biopolymer variants in the entire concentration range, the dilute and semi-dilute regions, was accomplished by plotting on a log-log scale the specific viscosity (η_{sp}) versus biosurfactants concentration (Fig. 1a). As visualized, there are two obvious areas in the curve, which were characterized by two different slopes in each curve. The first slope, in the dilute regime, showed a rather linear trend (*c* < *c**), where the individual polymeric chains are present as the separated coils, assigned to the line with a slope of ~0.9–1.4. As the biosurfactants concentration was increased, the specific viscosity remarkably increased as the separate chains become entangled with each other. The biopolymeric conformation upon the coil overlap is altered because the chains become progressively entangled. This concentration was considered as the biosurfactant coil-overlap concentration, and for acetylated starch, OSA starch, DS inulin, and EHEC it was found to be 3.6, 2.3, 1.8, and 1.4 g L^{-1}, respectively (Table 1).

At *c* < *c**, individual coils are separated and show small mutual interference, where the flow feature is Newtonian (Shahbazi et al., 2017). Beyond *c** (*c* > *c**), the entangled of biopolymeric chains progressively develops, causing the dynamics of chain relaxation to change from Rouse/Zimm type behavior to that described by the reputation model (Doi & Edwards, 1988). In the semi-dilute region, the macrostructure entanglement of a surface-active biopolymer is induced because of the chain-chain interaction (Shahbazi et al., 2017). Thus, the entangled polymeric chains, governed by reptation motions, result in conformational alteration due to increased chain interactions (Doi & Edwards, 1988). This could be more prominent in some functional properties of emulsion-containing biosurfactants such as in their consistency index, yield stress, and storage modulus, where the rheological parameters might be more affected by the surface-active biopolymers with lower *c**.

An appropriate indicator of the hydrodynamic volume of the biopolymeric coils is the limiting viscosity number or intrinsic viscosity ([η]). It is simply measured below the *c** (in the dilute region) of the biosurfactant (Morris et al., 1981). The values of [η] for each biosurfactant were obtained by the average intercepts of reduced and inherent viscosities (determined by Eqs. (4) and (5)), according to the method of Huggins and Kraemer, respectively. As can be seen from Table 1, the higher value of intrinsic viscosity was detected for EHEC with a value of 13.85 L g^{-1} and the lower one was related to the acetylated starch about 2.83 L g^{-1}. The intrinsic viscosity values for DS inulin and OSA starch were also determined to be about 8.38 and 5.34 L g^{-1}, respectively.

The zero-shear specific viscosity (η_{sp})$_0$ plotted versus the surface-active biopolymer concentration varies relates to the polymeric conformation and molecular weight based on the relating variations in the coil overlap (Doi & Edwards, 1988; Shahbazi et al., 2017). The double logarithmic curve of the coil-overlap parameter (by manipulating concentration in intrinsic viscosity), as indicated by *c* [η], against (η_{sp})$_0$ displays two distinct areas (Fig. 1b). The first one, referred to as the dilute region, is described by spatially separate individual coils of surface-active biopolymers, whereas the second region, termed the semi-dilute region, is encountered when the overall hydrodynamic volume of the separate chains is more than the volume of the solution. Therefore, in a semi-dilute regime, the chains have to overlap each
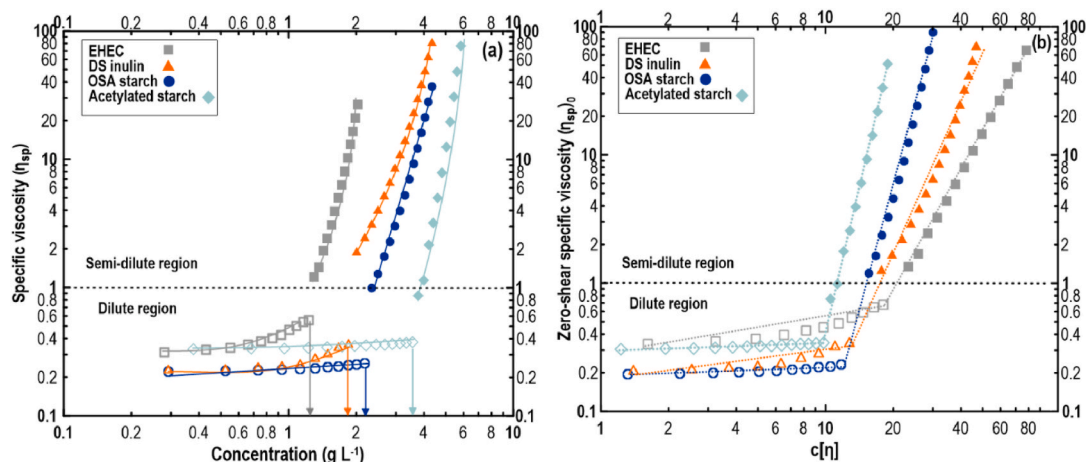
Fig. 1. Specific viscosity plotted against the concentration on a log-log scale (a) and coil-overlap parameter curve (b) biosurfactant verities. The hollow and solid symbols represent data in the dilute and semi-dilute regimes, respectively.

Table 1
Number- (Mn), weight- (Mw), Z-average (Mz) molecular weight, polydispersity index (DP), and radius of gyration (R_g), as well as intrinsic viscosity $[\eta]$, coil-overlap concentration (c^*), and critical coil-overlap parameters ($c^*[\eta]$) for biosurfactant variants determined by SEC-MALLS and capillary viscometer.

Biosurfactant type	Mn (g mol^{-1}) $\times 10^6$	Mw (g mol^{-1}) $\times 10^6$	Mz (g mol^{-1}) $\times 10^6$	DP (Mw/Mn)	R_g (nm)	c^* (g/L)	$[\eta]$ (L/g)	$c^*[\eta]$
Acetylated starch	0.54 ± 0.01^d	1.84 ± 0.01^d	2.74 ± 0.01^d	3.41 ± 0.31^b	27 ± 0.2^a	3.6 ± 0.03^d	2.83 ± 0.1^a	10.2
OSA starch	0.79 ± 0.01^c	2.25 ± 0.01^c	3.15 ± 0.01^c	2.85 ± 0.44^a	27 ± 0.1^a	2.3 ± 0.01^c	5.34 ± 0.2^b	12.3
DS inulin	1.12 ± 0.01^b	2.98 ± 0.01^b	3.73 ± 0.01^b	2.66 ± 0.32^a	42 ± 0.4^b	1.8 ± 0.01^b	8.38 ± 0.2^c	15.1
EHEC	1.28 ± 0.01^a	3.23 ± 0.01^a	4.48 ± 0.01^a	2.52 ± 0.24^a	58 ± 0.5^c	1.4 ± 0.01^a	13.85 ± 0.4^d	19.4

[a–d] Means (three replicates) within each column with different letters are significantly different ($P < 0.05$), Duncan's test.

other. The slope of the $(\eta_{sp})_0$ curves abruptly increase at a specific point (namely the critical coil-overlap parameter or $c^*[\eta]$), where the rise is much steeper with changes in the concentration (or coil-overlap parameter $c[\eta]$) of the polymeric emulsifier (Table 1). In the present work, the attained zero-shear specific viscosity for the biopolymeric surfactant at $c^*[\eta]$ was lower than that reported for random coil biopolymers (Morris et al., 1981). It was stated that the zero-shear specific viscosity of the random-coil polysaccharides has a $(\eta_{sp})_0$ of ~10 at the intersection point. In certain circumstances, the rigid modified biopolymers can be more effectively packed (Smidsrød & Haug, 1971; Shahbazi et al., 2017). Therefore, the lower values of $(\eta_{sp})_0$ concerning different biosurfactant variants at the point of $c^*[\eta]$ might be taken to imply a more rigid conformation of the biopolymeric structure. As an

important consequence, the biosurfactants with a higher value of intrinsic viscosity and a relatively lower critical overlap concentration might exert a substantial effect on the flow behavior, viscoelastic properties, structural strength, thixotropic feature, and emulsion stability, in which the higher mechanical strength and lower creep compliance may be obtained by the surface-active biopolymers with higher $c^*[\eta]$.

3.2. SEC-MALLS results of biosurfactants

Additional insights into the macromolecular properties were obtained by determining the molecular weights of the biosurfactant variants through SEC–MALLS (Fig. 2). By means of size exclusion
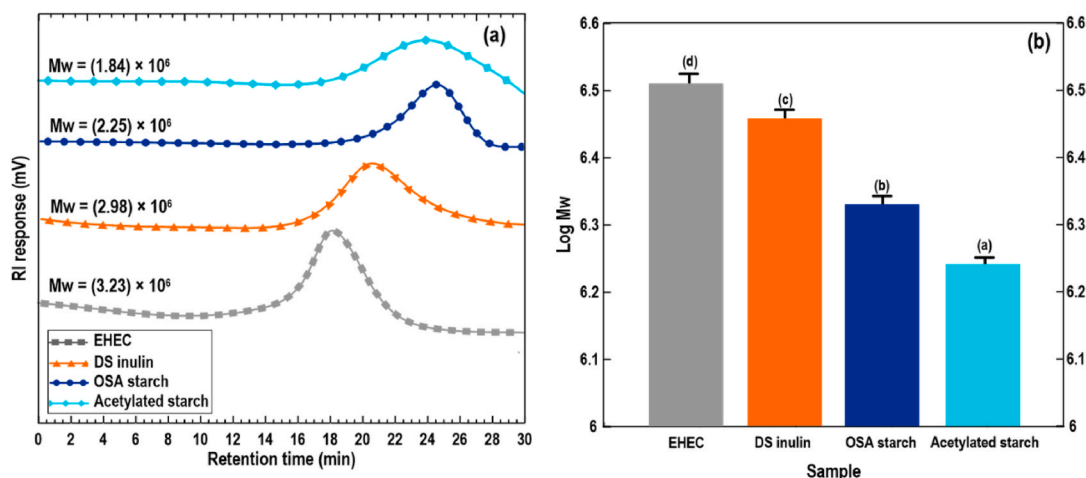
Fig. 2. SEC-MALLS chromatograms (a) and obtained log Mw (b) of biopolymeric surfactant variants. The means inside each column with various letters (a–d) are significantly different ($P < 0.05$) according to Duncan's test.

chromatography, biopolymers are separated based on their hydrodynamic volume, which is associated with the extension and swelling of the biopolymeric chains and their hydration conditions. Fig. 2a shows the molecular weight distributions of biopolymeric surfactant variants through elution profiles measured by SEC-MALLS. The relevant molecular parameters were also collected for all biosurfactants and the results are summarized in Table 1. Compared to EHEC and DS inulin, an increase of the retention time was obviously remarkable when injecting OSA starch and acetylated starch. Definitely, the biopolymers are retained longer in the columns owing to a reduction of their hydrodynamic volume (Yang & Zhang, 2009). Therefore, OSA and acetylated starches showed a lower average molecular weight (*Mw*) in comparison with EHEC and DS inulin (Fig. 2b). The SEC-MALLS data also verified the conclusions arrived in the previous section using intrinsic viscosity experiments.

Polydispersity index or *DP* (*Mw/Mn*) is a useful parameter to assess the molecular mass distribution of a biopolymer. A greater polydispersity index indicates a different molecular weight distribution which may result in a less functional gel network, yielding a lower structural strength. From Table 1, the *DP* was found to vary between 2.52 and 3.41, with the higher value of *DP* obtained for acetylated starch and the lowest one for EHEC. An increased *DP*, together with a decreased *Mw*, may lead to a decrease in viscosity and lower emulsion stability, which can also be associated with decreasing dynamic storage moduli of the fabricated emulsions.

Table 1 also presents obtained data regarding the radius of gyration (*Rg*) for biosurfactant variants. In general, the *Rg* depicts the mass average (root mean square) distance of each point in a molecule from the molecule's center of gravity, which is related to the actual space that was occupied by the chain (Yang & Zhang, 2009). The higher value of *Rg* was

obtained for EHEC with a value of 58 nm, followed by DS inulin with an *Rg* of 42 nm. The *Rg* values for OSA starch and acetylated starch were also obtained to be 27 nm. Therefore, EHEC and DS inulin might adsorb faster and cover the oil droplet surfaces better than OSA and acetylated starches (Bai, Huan, Li, & McClements, 2017).

3.3. Rheological properties of SPI-based inks

3.3.1. Steady rheological properties

In extrusion-based 3D printing, printable inks must easily flow through a nozzle tip, and should also possess enough mechanical strength to develop and retain well-defined geometries. However, the inks with high mechanical strength are always characterized by high viscosity and large yield stress, which could simply block the nozzle tip and lead to a time-consuming cleaning procedure or even damaging the whole of a typical print-head (Shahbazi & Jäger, 2020; Shahbazi et al., 2021a). To address this problem, inks with strong shear-thinning and desirable viscoelastic behavior are required as they could be easily extruded out through the nozzle, with the application of a reasonable extrusion shear force (Chen et al., 2019; Shahbazi & Jäger, 2020). Fig. 3 shows the influence of oil replacement by different levels of biosurfactants on the variation of stress-strain curves of the SPI-based ink. Rheological data showed all emulsions containing biosurfactants exhibited shear-thinning behavior (*n* < 1) (Tables A.1–A.4 in Supplementary Materials). In this regard, the values of yield stress (τ_0), consistency index (*K*), and flow behavior index (*n*), presenting a good fit to the Herschel-Bulkley model with high correlation coefficients (R^2) above 0.98. These results have been supported by other works in the meat emulsion systems stabilized by different hydrocolloids (Wang et al., 2020; Wang, Wang, & Adhikari, 2011).
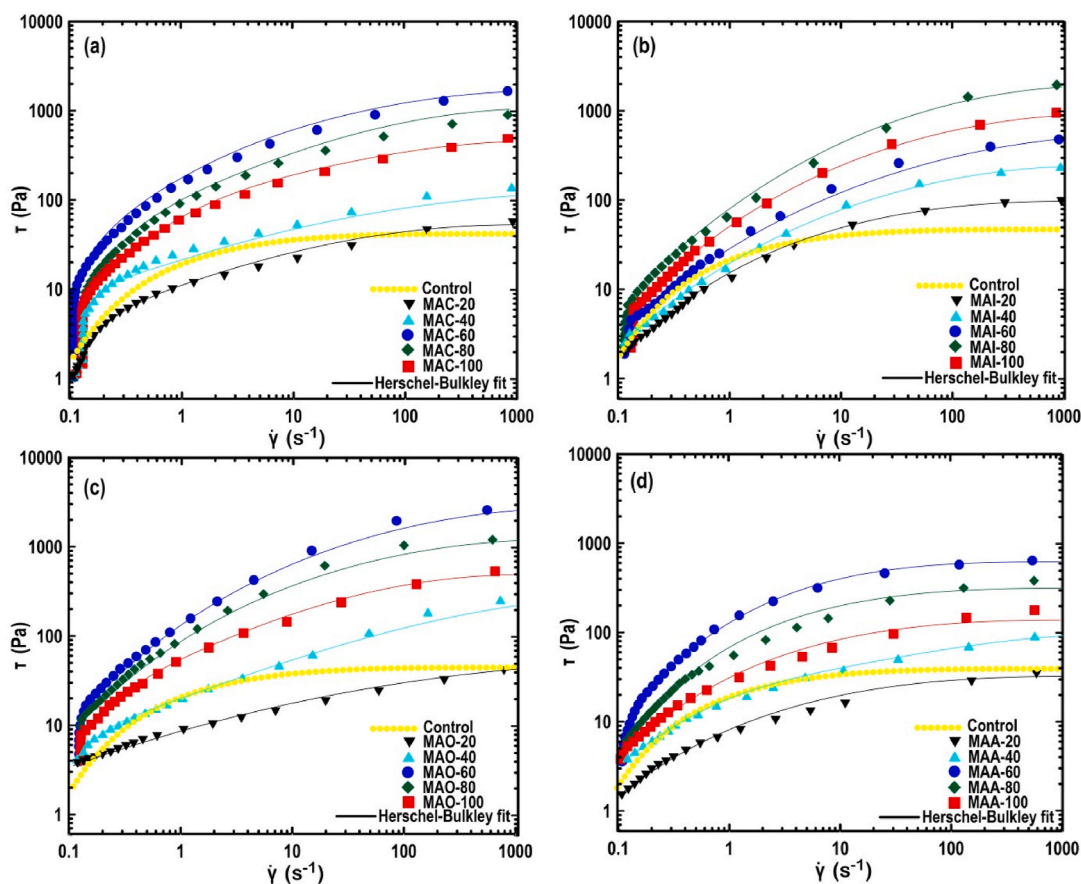
Fig. 3. Changes in shear stress-shear rate curve of SPI-based ink as a function of substitution of oil by different levels of EHEC (a), DS inulin (b), OSA starch (c), and acetylated starch (d).

Fig. 3 shows that control SPI-based ink exhibited *pseudoplastic* behavior over the entire shear rate range (0.1–1000 s^{-1}) with consistency index and flow index of 31.9 Pa s and 0.84, respectively (Table A.1 in Supplementary Materials). The effect of EHEC replacement on the rheological behavior of SPI-based ink is observed in Fig. 3a and data are given in Table A.1. The ink containing 20% EHEC overall exhibited lower yield stress, consistency index (indicating the ink became less viscous), and a higher flow behavior index (i.e., less shear-thinning) than those of samples containing a higher EHEC ratio ($P < 0.05$) (Table A.1 in Supplementary Materials). This result might be related to an inadequate ratio of EHEC to complete oil droplets coverage, and also poor steric or electrostatic repulsion among droplets to avoid droplet aggregation, leading to large flocs and coalescence development (Dickinson & Galazka, 1991; Shahbazi et al., 2021a). In contrast, with increasing EHEC ratio up to 60% yield stress and consistency index gradually increased and flow behavior index decreased (representing the ink became more shear-thinning) likely due to the promotion of a gel-like network in the ink (Genccelep, Saricaoglu, Anil, Agar, & Turhan, 2015). This suggests that in the presence of a higher ratio of EHEC, the droplets in the ink-based emulsion were less aggregated and more effectively dispersed. This effect might also be related to an increase in the total solids content and/or the interactions between hydrophilic/hydrophobic groups of EHEC with SPI and oil phases, respectively (Tadros et al., 2004; Tadros, 2009). However, beyond the 60% EHEC ratio, the ink consistency index decreased as a result of a reduction in the oil phase fraction. It was stated that a decrease in the packing fraction of oil droplets and with a weakly flocculated system, the yield stress is not sufficient and the system simply collapses under its own weight (Dickinson, 2012).

Regarding SPI-ink formulated by modified DS inulin, rheological data revealed the ink became more viscous (increasing the consistency index) and more shear-thinning (decreasing the flow behavior index) with an increase in modified inulin ratio up to 80% (Table A.2 in Supplementary Materials). A higher DS inulin ratio might simplify the adsorption of alkyl groups at the interface, thus to some extent increasing the effective size of oil droplets, subsequently improving consistency index (Tadros et al., 2004; Kokubun, Ratcliffe, & Williams, 2018). There was also an SPI/DS inulin interaction related to the free hydrophilic groups of the adsorbed biosurfactant molecules and SPI. In contrast, the consistency index and yield stress of MAI-100 showed a lower value with a higher flow index compared to MAI-80 (Fig. 3b), which could suggest that a loss in the oil phase volume fraction as a result of the total substitution of oil by DS inulin (Sun & Gunasekaran, 2009).

The consistency and flow behavior indices, as well as yield stress of the SPI-based inks formulated with 20% OSA- and acetylated starches, were decreased in comparison with control ink, which might be ascribed to a lower concentration of free biosurfactants to cover the oil droplets (Tables A.3 and A.4 in Supplementary Materials). Free biosurfactant has an appreciable influence on the rheological properties of emulsions (Tadros, 2009). In contrast, an increasing ratio of OSA and acetylated starches up to 60% led to higher yield stress and consistency index of SPI-based ink emulsion (Figs. 3c and d). This might be related to an increase in biosurfactant level in the system, which is accountable to initiate the individual biopolymeric coil overlap and development of intermolecular junctions in the emulsion; therefore, arrangement and elongation of biopolymeric chains could be limited by the increasing ratios of OSA and acetylated starches (Prochaska, Kędziora, Le Thanh, & Lewandowicz, 2007). Further increase in the ratio of hydrophobically modified starches up to 80 and beyond 100%, led to a decrease in consistency index and yield stress. This might be assigned to the lowered amount of packing of oil droplets in the systems at the lower oil ratio, where there is a restricted contact surface region among oil droplets to oppose the free flow of the ink system in a shear field; therefore, decreasing its viscosity. Similar results were reported for emulsions stabilized by SPI (Tang & Liu, 2013), whey protein isolate–xanthan gum mixture (Sun & Gunasekaran, 2009), and pre-heated whey protein (Liu & Tang, 2011).

3.3.2. Strain sweep

An ideal ink for the 3D printing process should demonstrate *pseudoplasticity* as it could simply be extruded out from a nozzle tip with the application of a reasonable extrusion shear force. However, a suitable viscoelastic ink with desired mechanical strength, which is specified by the value of G', is essential to support the designed structure and preserve the printed architectures. This is particularly useful for those 3D constructs with complex structures and twisting challenges, like the development of complex shapes and geometries with intricate designs (Shahbazi & Jäger, 2020). The purpose of the strain sweep assay was to determine the strain limit of LVR in the prepared inks for upcoming frequency sweep evaluation. The mechanical spectrum for control SPI-based ink indicates that the G'_{LVR} value prevailed over the loss modulus (G''_{LVR}) (Fig. 4); accordingly, a gel-like network was detected. Moreover, at the higher shear strains (>1%), G' drastically decreased once strain increased, indicating a structural weakening and/or breakdown of the emulsion matrix. As visualized from Fig. 4, the oil replacement by all biosurfactants in all ratios, except 20%, caused a notable increase in the G' parameter of printable inks. This is in accordance with previous reports about the influence of biopolymeric surfactant on the rheological properties of meat emulsions (Genccelep et al., 2015). This indicates that the reduced-fat inks exhibited a more elastic character inside the LVR, specifying that biosurfactants replacement led to an increase in the resistance of the ink to any deformation. The adsorption of the biosurfactant variants at the oil droplet interface was likely facilitated through higher ratios of surface-active biopolymers, increasing the oil droplet number density, and therefore improving elastic modulus.

The higher G' values in the inks containing EHEC and DS inulin might be ascribed to their higher radius of gyration (effective volume) or chain associations resulting from the hydrophobic attraction between grafted ethyl (hydroxyethyl) and dodecenyl succinylate groups with oil and hydrophilic backbones of biopolymers interacting with polar groups of soy protein. From this point of view, the printable inks with higher G' and stronger mechanical strength (as well as yield stress) might self-support their own weight upon the 3D printing process (Shahbazi et al., 2020). Mechanical spectra also showed that further increase in biosurfactant concentration and a simultaneous decrease in oil ratio (100:0%), corresponded to a decrease in the G'. Again this suggests that the oil-free inks have fewer stable structures, thanks to total oil substitution by surface-active biopolymers.

Fig. 4 also revealed the extent of LVR, in which the viscoelastic variables are independent of the strain amplitude. These became broader upon oil replacement by surface-active biopolymers in the ratio range of 40–80%, suggesting greater mechanical stability of the viscoelastic inks under the strain amplitude (Kiumarsi et al., 2021). The extent of LVR is an indicator of structural stability and shape preservation ability against the application of stresses causing mechanical deformation (Shahbazi et al., 2020). The current results could be explained by the greater degree of interaction among the hydrophilic/hydrophobic domains in the reduced-fat emulsions (inks with 40–80% biosurfactants), which consequently caused the formation of more structured and mechanically stable systems. Among all studied ink-based emulsions, the sample formulated by EHEC showed a longer LVR length with a greater G' value (Fig. 4a), followed by ink containing DS inulin (Fig. 4b). In contrast, inks prepared with OSA starch (Fig. 4c) and acetylated starch (Fig. 4d) presented a more limited LVR. This indicates an improvement in the structural strength of MAC and MAI inks, most likely due to the higher intrinsic viscosity and $c*[\eta]$ provided by EHEC and DS inulin. This may contribute to fabricating 3D printed architectures with well-defined geometries and improved mechanical strength.

On the other hand, the G'' parameter showed a maximum at higher
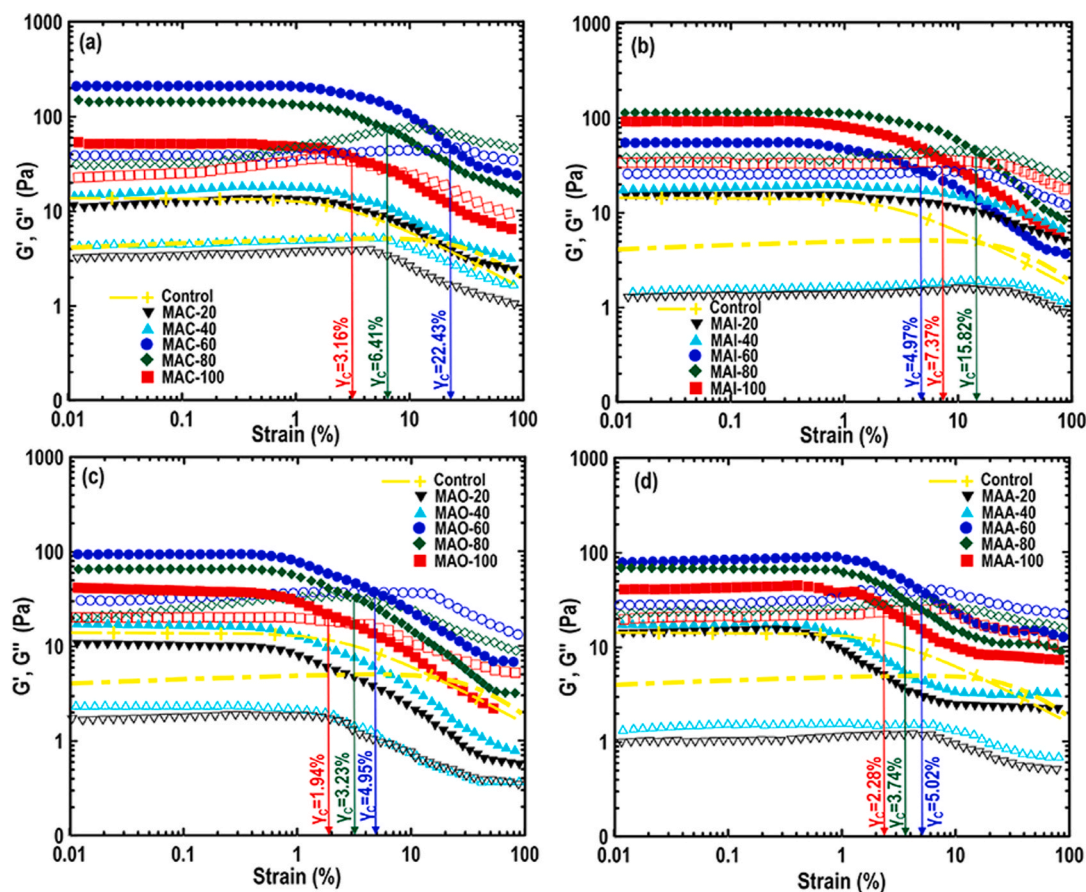
Fig. 4. Changes in elastic modulus (solid symbols) and viscous modulus (hollow symbols) as a function of strain for inks formulated with different ratios of (a): EHEC, (b): DS inulin, (c): OSA starch, and (d): acetylated starch. The γ_c represents the crossover point. The linear viscoelastic limits are indicated by arrows.

strains (>1%), whose amount crossed over with that of G' (i.e., $G' = G''$) for inks containing 40–60% biosurfactants (Fig. 4). The peak in G'' indicated maximum energy dissipation (viscous response) and the moduli crossover implied a transition from viscoelastic solid-like to viscoelastic liquid behavior (Shahbazi et al., 2020). A shift in the crossover point to the higher strains was also found for MAC-60, MAI-80, MAO-60, and MAA-60. After that transformation, the continued reduction of G' and G'' showed the stiffness of ink structures reduced with increasing the strain amplitude. The existence of a maximum in loss modulus was categorized as type III behavior (weak strain overshoot) (Hyun, Kim, Ahn, & Lee, 2002). This phenomenon has been stated in structured emulsions, soft glassy compounds, entangled biopolymeric systems, and associative biopolymeric dispersions (Hyun et al., 2011). At the low deformation rates, the intermolecular interactions are in dynamic equilibrium and the network acts as a viscoelastic solid. As the strain amplitude rises, the degradation of structure occurs more quickly compared to its reformation rate (i.e., elastic element reduces) and the system displays increased viscous fluid behavior. Of course beyond LVR the absolute values of G' and G'' need to be treated with some caution since the response of the system is no longer linear. Nonetheless, the fact that the value decrease is a good indication of a changing (breakdown) of any stress-supporting structure/network in the system. In this scenario, a maximum in G'' indicates the point at which an adequate extent of such stress-supporting structure is degraded to transform the gel-like system into a viscous fluid. As a result, an ideal printable ink should be able to preserve the shape upon extrusion shear force and are capable of fusing with formerly printed layers. Therefore, an improvement in the strength of emulsion gels offered by surface-active biopolymers might be valuable for reduced-fat inks to easily extruded out from the nozzle tip.

3.3.3. Frequency sweep

The frequency sweep assays were carried out in the linear viscoelastic regime to further investigate the microstructural changes and the presence of networks in SPI ink, upon surface-active biopolymers substitution. The G' and G'' moduli of the inks formulated by biosurfactant variants are presented in Fig. 5, plotted as a function of angular frequency (ω). Irrespective of biosurfactant type, the G'_{LVR} values of inks were always higher than those of the G''_{LVR}, which demonstrated they have an elastic character rather than a viscous feature. Hence, the inks could be described as a solid-like system with gel-like properties. The relevant results were previously reported for different meat emulsions including biosurfactants (Flores, Giner, Fiszman, Salvador, & Flores, 2007; Genccelep et al., 2015). Fig. 5 also demonstrates that increasing ratios of biosurfactant allowed an increase in G', with more noticeable impact at the ratios of 40–80%, implying oil replacement with surface-active biopolymers contributed to the viscoelastic properties with an improvement in the structural strength. This was perhaps not surprising, since there are more hydrophobic/hydrophilic groups present with the higher ratios of surface-active biopolymers, able to interact with comparable groups in the adjacent droplets, enabling the promotion of a gel-like network in the system. The biosurfactants contribute to the mechanical stability of inks and a more desired gelation dynamics, since they are effective concerning their molecular weight and providing numerous active binding sites at the oil-water interfaces. It was also proved the inter-droplet attractive interaction forces principally accounted for the gel-like network formation, with higher mechanical stability at the higher biosurfactant level (Tang & Liu, 2013). However, beyond 60 or 80%, G' was notably lower, most likely owing to a reduction in the packing fraction of oil droplets, and a loss in the gel network structure because of a higher substitution of oil by
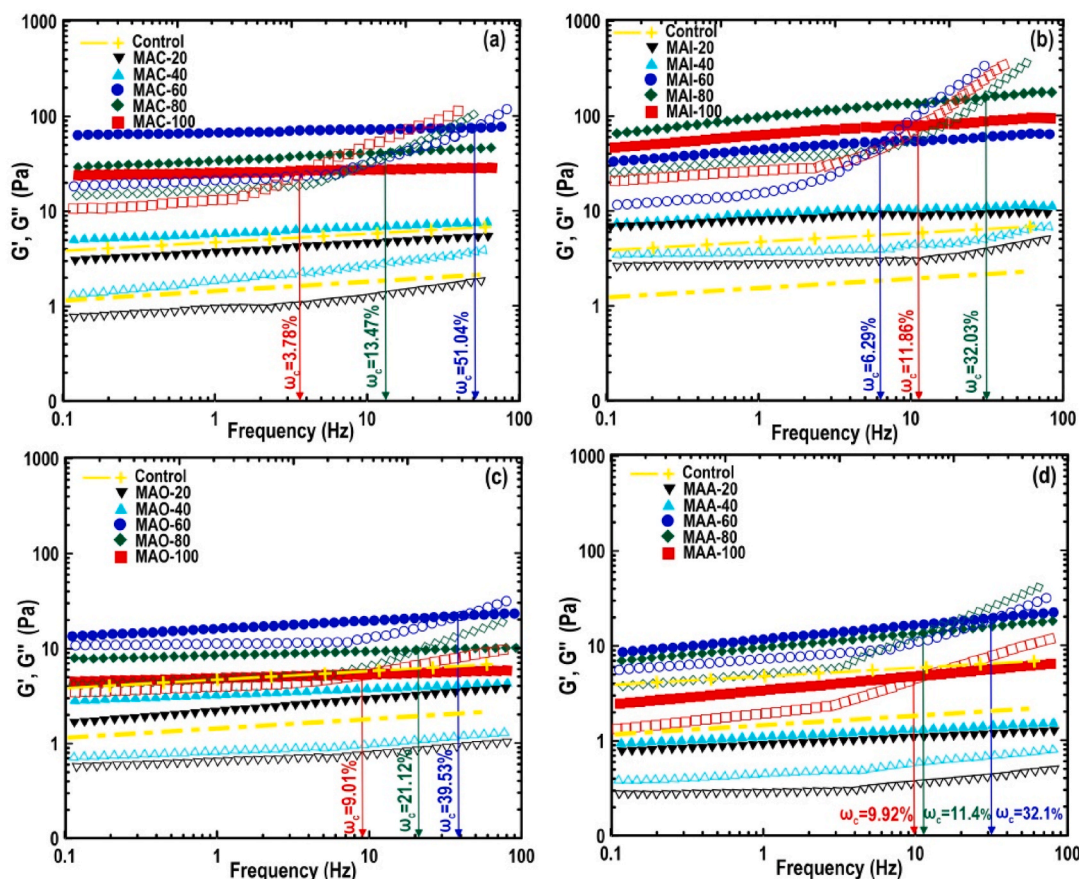
Fig. 5. Storage modulus, G' (solid symbol) and loss modulus, G'' (open symbol) of SPI ink as a function of frequency for inks with different levels of (a): EHEC, (b): DS inulin, (c): OSA starch, and (d): acetylated starch. The ω_c denotes the crossover point.

biosurfactants (Dickinson, 2012).

Fig. 5 also displays that the viscoelastic properties of SPI-based inks, prepared with 40–80% biosurfactants, greatly vary with frequency. In these cases, dynamic moduli exhibited a crossover (ω_c), where the inks showed a dominant solid-like system below the crossover frequency ($G' > G''$) and more of a viscous fluid behavior above it ($G'' > G'$), implying the change in the response of the system from a more gel-like to a liquid-like behavior, as greater energy dissipation takes place at these intermediate frequencies. Moreover, increasing biosurfactant ratio shifted the ω_c point to the higher frequencies, where MAC-60 (Fig. 5a), MAI-80 (Fig. 5b), MAO-60 (Fig. 5c), and MAA-60 (Fig. 5d) showed the highest ω_c value. This indicated the development of more structured and connected networks with inks behaving as elastic gel-like systems (Fig. 5). The formation of the viscoelastic systems with higher biosurfactants levels might have benefits for a 3D printed architecture to retain its shape over time and achieve higher resolution during printing, hence improving the texture and sensory attributes of fabricated reduced-fat products. Furthermore, the fact that some of the oil droplets were trapped inside biosurfactant microparticles, especially at the higher ratios, may have a desirable influence on the flavor descriptions of reduced-fat samples (Malone & Appelqvist, 2003). Based on the dynamic rheological behavior it could be concluded that SPI-based inks with different biosurfactants demonstrated different structural strength. The EHEC and DS inulin considerably enhanced the G' of the ink system possibly because of greater intrinsic viscosity or molecular weight. Therefore, higher mechanical strength may allow reduced-fat inks to better hold their shape and offer mechanical stability upon printing, which is especially beneficial in the 3D printing application.

3.4. Creep-recovery and 3-ITT measurements

The creep and 3-ITT experiments are an efficient tool to conduct prompt stress and deformation, respectively, to mimic the impacts of extrusion shearing force upon 3D printing and also handling steps of 3D printed objects. The creep-recovery tests can be used to evaluate the transient behavior of the viscoelastic properties of ink dispersion. When a viscoelastic material is subjected to prompt and constant stress, the deformation rises over time, and the consequent elimination of stress results in a reduction in the strain. This behavior directly relates to the material viscoelastic features, which might or might not reach zero deformation over time. The creep and creep-recovery compliance of printable ink variants presented the viscoelastic response of microstructure to constant applied shear stress and removal (Fig. 6). The creep-recovery curve provides several parameters, however, in the current study, maximum $J(t)$ (the peak deformation in the completion of creep phase) and relative recovery (the deformation recovered at the end of the recovery phase, divided by the peak deformation) parameters were extracted. A lower peak deformation specifies a stiffer structure with lower flowability (Shahbazi et al., 2021a). The printable inks prepared with biopolymeric surfactants showed similar trends, that is, lower $J(t)$ magnitudes in the creep region were obtained by greater ratios of biosurfactant variants. This suggests the development of reinforced SPI-based ink structure induced by biosurfactant replacement. In general, the $J(t)$ values of inks prepared with EHEC and DS inulin were lower than those of corresponding inks prepared with OSA and acetylated starches. As visualized from Figs. 6a and b, the peak strain for MAC-60 and MAI-80 ($J(t) = {\sim}0.012$ Pa^{-1}) was 75-fold lower than the control ink ($J(t) = 0.9$ Pa^{-1}). Thus, it seemed that EHEC and DS inulin could more increase the elastic elements of the viscoelastic feature likely
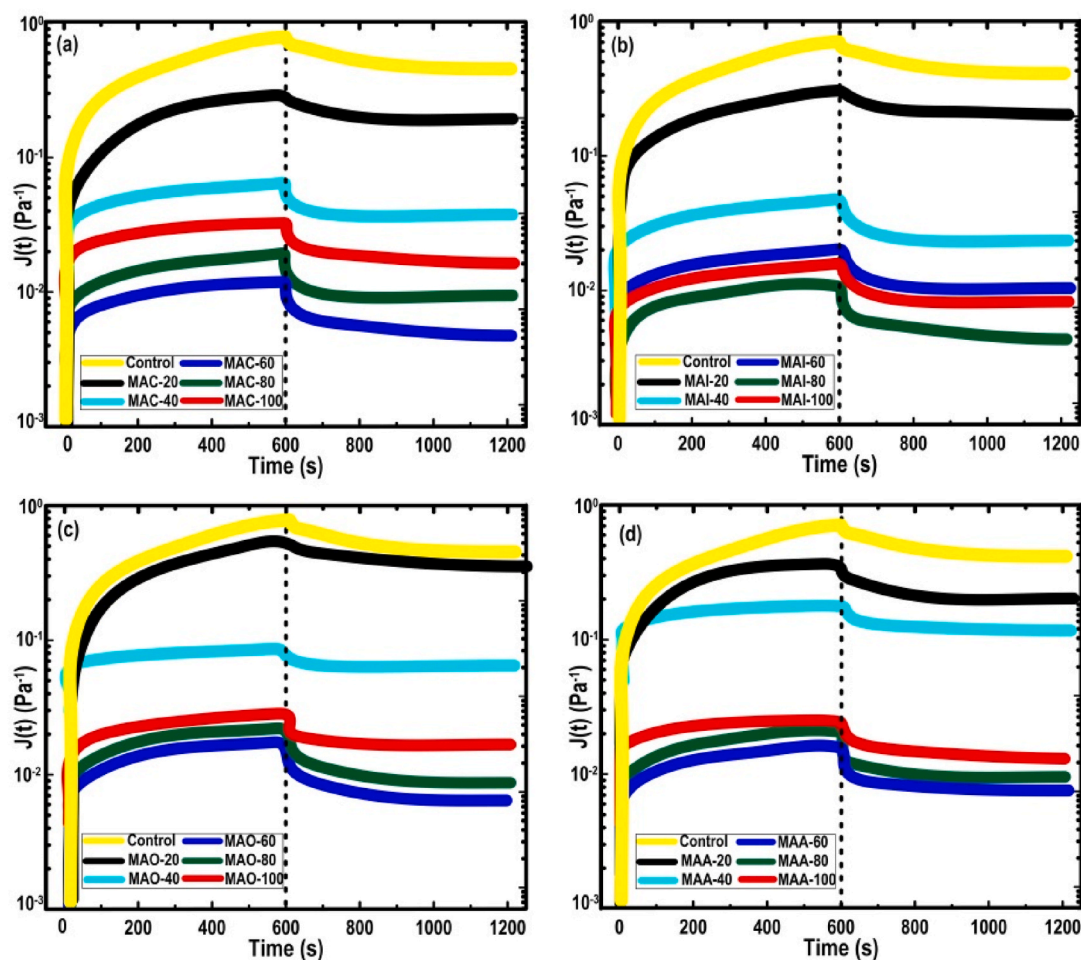
Fig. 6. Creep curves of the SPI-based inks as influenced by oil replacement by different levels of (a): EHEC, (b): DS inulin, (c): OSA starch, and (d): acetylated starch.

due to higher coil-overlap parameters and greater compact conformation. Compared to MAC-60 and MAI-80, a relatively softer structure of MAO-60 ($J(t) = 0.020$ Pa^{-1}) and MAA-60 ($J(t) = 0.019$ Pa^{-1}) could be interpreted from a comparatively higher peak strain and equilibrium strain amounts (Figs. 6c and d). These outcomes are in accordance with the data obtained from oscillatory experiments. The recovery phase of the creep experiment is the extent of the reduction of material deformation once the stress is eliminated. A greater relative recovery is related to a higher elasticity and a solid-like structure (Menard & Menard, 2006). The relative recovery capacity was increased with the increased ratio of biopolymeric surfactant in the ink-based emulsion. The recovery percentages of inks formulated by EHEC and DS inulin were larger than those fabricated with OSA and acetylated starches, offering an effective improvement of the ink system recovery (viscoelastic solid). A superior relative recovery of about 97% (Fig. 6a) was detected for MAC-60 as compared to 91% for MAI-80 (Fig. 6b), proposing a more stable MAC-60 structure with improved elasticity. Here, the grafted ethyl on the EHEC backbone might strongly interact with oil in ink-based emulsion and its hydrophilic domain effectively interacted with the polar groups of SPI, which might have a larger contribution to the elastic component of the viscoelastic system. When comparing the relative recovery of inks prepared by MAO and MAA (Figs. 6c and d), the ink-based emulsion formulated with a proportion of 60% MAO or 60% MAA showed the highest relative recovery in their clusters with recovery percentages of 70% and 72%, respectively. As an important consequence, the results of creep-recovery experiments offered the biopolymeric surfactant type and ratio influenced the elastic and the viscous components of the viscoelastic behavior in SPI-based ink, whose

outcomes agreed well with the results of previously discussed oscillatory measurements.

The structure recovery feature was also studied through evaluating 3-ITT, in which the change in the viscosity was detected as a function of time upon alternative low and high shear rate intervals. A thixotropic printable ink is extremely desirable for the extrusion printing process (Shahbazi et al., 2021a). In this sense, the 3-ITT experiment is an efficient means to conduct instantaneous deformation to mimic the impacts of extrusion shear force during printing and also handling steps of 3D printed objects. Preferably, materials are offered a desired thixotropic recovery if the peak viscosity in the third interval recovers at least 70% of its extent measured after the first interval (Menard & Menard, 2006). The viscosity profiles of printable ink variants as a function of time and shear rate application are shown in Fig. 7. Generally, there is a progressive increase in the viscosity of the inks prepared with a higher ratio of biosurfactants, displaying an increase in the structural strength. For the first shearing interval, MAC-60, MAI-80, MAO-60, and MAA-60 displayed a considerably higher viscosity in comparison with their counterparts. Concerning the third step, the viscosity of the ink-based emulsion variants was notably lower than those for the first step. In the 3-ITT experiment, once the shear rate abruptly steps up or down, the consequent viscosity transients reflect changes in the structure of systems under well-controlled flow conditions. Accordingly, the viscosity for ink-based emulsion under stepwise shear rate was related to its recovery compliance and viscoelasticity. Upon application of shearing in the second interval, some extent of interconnected structure in inks was broken, leading to an abrupt reduction of viscosity. Once came to the reversible restructuration (i.e., third interval), the polymeric backbone
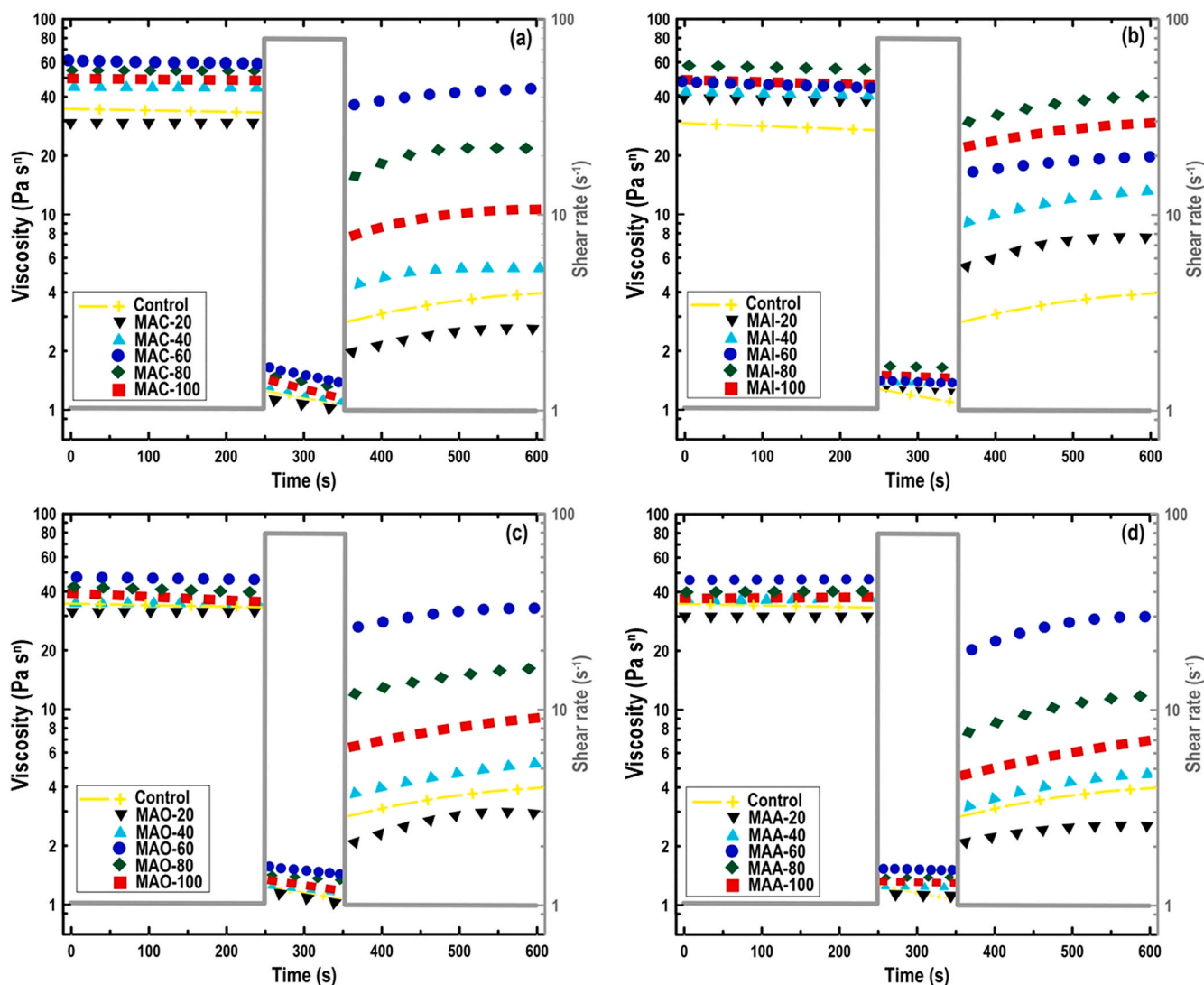
Fig. 7. Viscosity plot from 3-ITT of printable inks prepared with different ratios of (a): EHEC, (b): DS inulin, (c): OSA starch, and (d): acetylated starch.

rearranged as the structure came to the new equilibrium state, recovering its original structure. The printable inks of MAC-60 (Fig. 7a), MAI-80 (Fig. 7b), MAO-60 (Fig. 7c), and MAA-60 (Fig. 7d) revealed greater structural recovery compared to their counterparts, whose initial viscosity recovery values were measured to be 82%, 75%, 70%, and 74%, respectively. This might be ascribed to the fact that biosurfactants replacement at the higher levels led to the reinforcement of structure, offering the system resistance to the instant deformation. In contrast, the lower values of viscosity in the printable ink formulated with the lower biosurfactant ratio might be due to irreversible structural damage, where they showed a soft matrix because of the existence of less structured systems with low connected structure. These outcomes were consistent with the steady flow data and oscillatory measurements, where the more structured ink system exhibited a strong gel-like structure. The results, consequently, indicated that the MAC-60, MAI-80, MAO-60, and MAA-60 ink networks were dynamic and recoverable and thus, their appropriateness might be considered to process via 3D extrusion printer as a restoration network with reversible structure breakdown are highly desired.

3.5. Droplet size

The influence of particle size distribution on ink functionality is well established (Wu et al., 2016; Lee, Won, Kim, & Park, 2019). It has been reported that reduction in particle size of ink dispersion increases the ink functionality with consideration of improving the resolution of deposited layers, printing precision, and consequently, developing a well-defined geometry (Wu et al., 2016; Lee et al., 2019). The droplet sizes for SPI-based ink obtained from biosurfactant variants at different ratios were monitored over time to evaluate their efficiency on ageing (Fig. 8). Regarding EHEC, the ($d_{3,2}$) and ($d_{4,3}$) diameters for MAC-20 and MAC-40 increased upon the 21 days (Fig. 8a). In the presence of a low concentration of surface-active biopolymer, most of the separate droplets developed through the extreme energy dissipation were not maintained in final ink (Dickinson & Galazka, 1991), leading to larger droplet sizes. However, the ($d_{3,2}$) and ($d_{4,3}$) for MAC-60 remained comparatively constant over the 21 days with smaller droplet sizes, showing the coalescence and/or flocculation did not happen. In this context, an increase in the viscosity of the continuous phase offered the stabilizing effect of EHEC on SPI-based ink. Moreover, it has been proposed the existence of intermolecular interactions between hydrophilic/hydrophobic groups in the system contributes to biosurfactant effectiveness on aging (Dickinson & Galazka, 1991). The ($d_{3,2}$) and ($d_{4,3}$) for the ink-based emulsions prepared using 20–60% modified DS inulin exposed there was an increasing trend in the droplet size (Fig. 8b), which might be assigned to the division of adsorbed layer among adjacent droplets (flocculation). In contrast, modified DS inulin at the level of 80% produced an ink with smaller droplet sizes, in which there was no
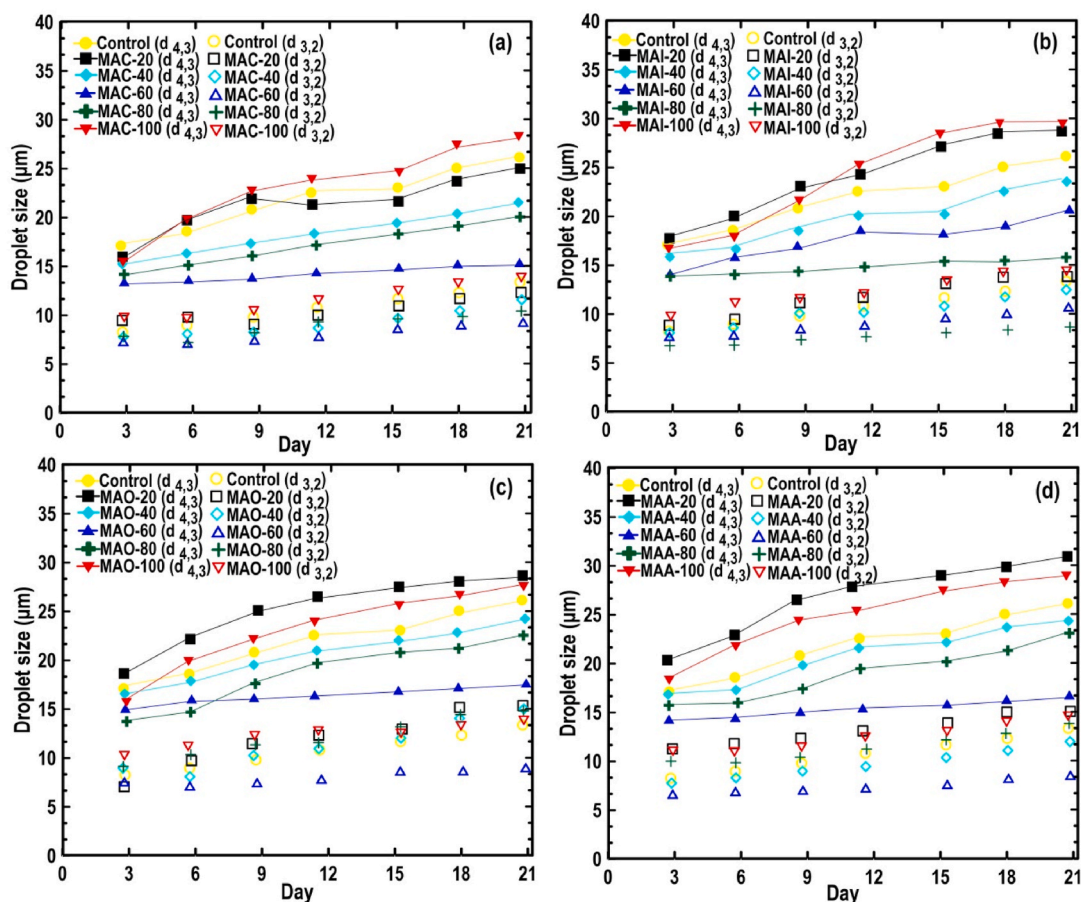
Fig. 8. Droplet size for SPI-based inks prepared with various with different levels of (a): EHEC, (b): DS inulin, (c): OSA starch, and (d): acetylated starch.

change detected in the $(d_{3,2})$ and $(d_{4,3})$ upon storage for 21 days. This result is in accordance with the study by Kokubun et al. (2015), who reported the hydrophobically modified inulin yielded emulsions with smaller droplet sizes and more uniform distribution. The emulsion stability of MAI-80 might be related to strong attractive interaction forces offered by a higher modified inulin ratio. This may arise due to the presence of the amide protein and aldehyde head groups, on one hand, and the interaction of the alkyl domain with the oil phase.

The droplet sizes for inks prepared using OSA and acetylated starches are also illustrated in Figs. 8c and 8d, respectively. The $(d_{3,2})$ and $(d_{4,3})$ droplet diameters for the inks prepared using modified starches at the ratio of 20% and 40% increased remarkably and an emulsion instability was noted upon 21 days. The adsorbed layer thickness of biopolymeric surfactants was possibly inadequate to offer stability via steric repulsions, showing molecules need to provide somewhat flat conformation at the interface (Kokubun et al., 2015). In contrast, the $(d_{3,2})$ and $(d_{4,3})$ remained almost constant regarding the inks made by 60% modified starches. This proposed in the presence of a higher ratio of modified starches, the droplets were more effectively dispersed and less aggregated in the systems. An increase in the biosurfactant concentration might promote the initiation of separate molecules overlap and inducting a gel-like network, enabling the hydrophobically modified starches to efficiently stabilizes the ink-based emulsions. Nevertheless, beyond the 80% modified starches ratio, there was an increasing trend in the size of droplets upon storage for 21 days. The observed emulsion instability concerning these inks (i.e., MAO-80, MAO-100, MAA-80, and MAA-100) is likely because of the high affinity of modified starches to interact with comparable molecules in the adjacent droplets and ultimately coalescence to decrease the surface energy.

Fig. 9 shows the particle size distribution (PSD) of SPI-based ink

emulsions as influenced by the different ratios of biosurfactant variants. The PSDs for MAC-60 (Fig. 9a), MAI-80 (Fig. 9b), MAO-60 (Fig. 9c), and MAA-60 (Fig. 9d) inks were more uniform when compared with their corresponded samples, proposing better emulsion stability. Furthermore, the distribution was monomodal, presenting no stable flocs were identified upon the PSD experiment (Thanasukarn, Pongsawatmanit, & McClements, 2004). It could also be seen the PSD data were in agreement with results of $(d_{3,2})$ and $(d_{4,3})$. The better emulsifying capacity obtained by the higher ratio of biosurfactants might be due to the presence of more hydrophobic groups, the main responsible for their emulsifying. Therefore, grafted ethyl (hydroxyethyl), dodecenyl succinylate, OSA, and acetate groups on the cellulose, inulin, and starches backbones, respectively, could mostly interact with oil and more polar biopolymeric chain ends interacting mainly with the hydrophilic groups. This offers essential interfacial free energy reduction to prevent phase separation and system destabilization. Besides, the reduced droplet size and improved homogeneity with increasing the biopolymeric surfactant ratio were probably due to an increase in the oil droplets surface coverage, expressing as interfacial biosurfactant concentration. This result supports the above interpretation that the stabilizing effect of surface-active biopolymers is either due to an increase in viscosity of the continuous phase and/or the surface activity of the modified biosurfactants.

3.6. Confocal laser scanning microscopy (CLSM)

The network microstructure and interfacial framework in the continuous phase of the SPI-based ink were obtained through CLSM (Fig. 10). Additionally, droplet size distributions determined using light scattering were superimposed on the fluorescence images to highlight
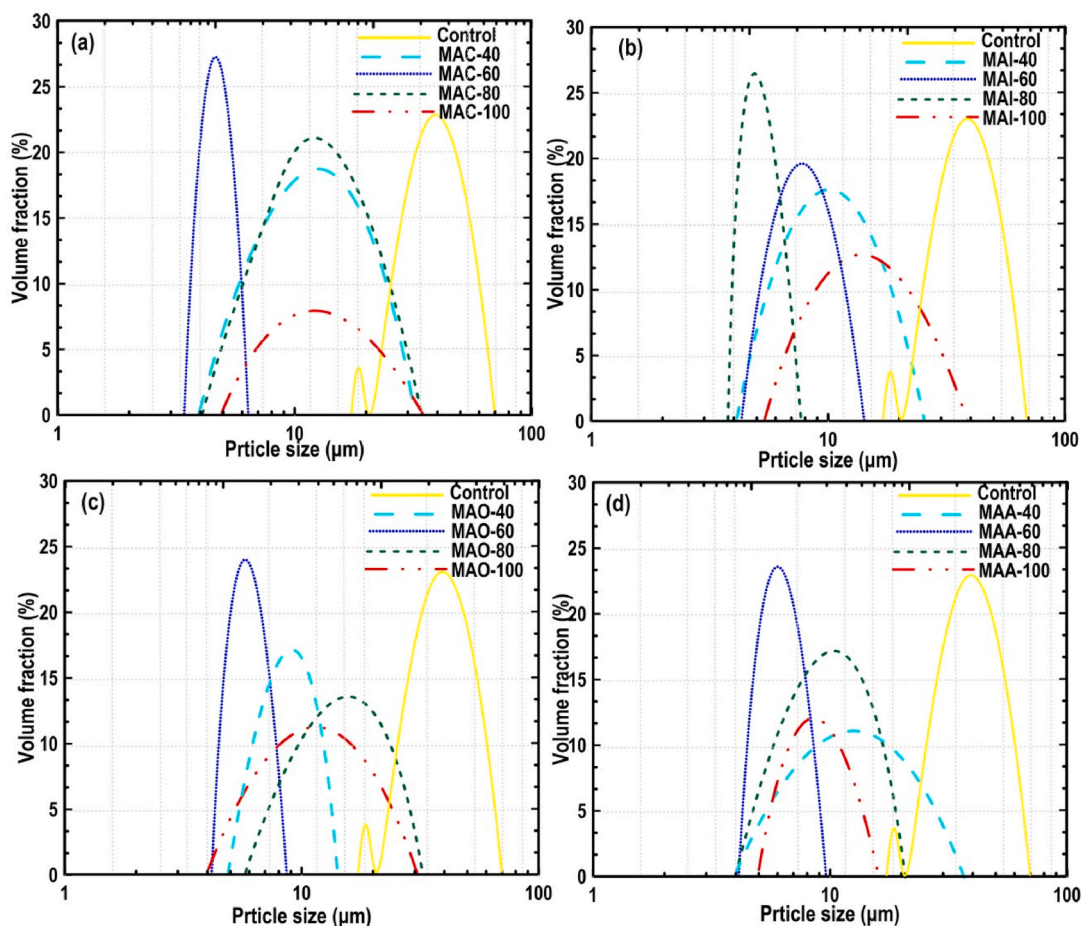
Fig. 9. Influence of biosurfactant variants concentration on particle size (μm) distribution of SPI-based ink emulsions prepared with different ratios of (a): EHEC, (b): DS inulin, (c): OSA starch, and (d): acetylated starch.

the correlations among microstructure and particle size distribution. The possibility to combine CLSM with light scattering and other physical analytical techniques in the same experiments with specially designed stages allows obtaining detailed structural information of complex systems (Shahbazi et al., 2021b). Since MAC-60, MAI-80, MAO-60, and MAA-60 inks presented better emulsion stability, lower creep compliance, greater structural recovery, and improved rheological parameters, the microstructures of these samples were imaged. In the absence of biosurfactants (control sample), the oil droplets seemed big and there were rather small spaces between them (Fig. A.3 in Supplementary Materials). This instability might be due to the lack of surface-active biopolymers present at the created oil/water interface for surface coverage. Thus, coalescence and flocculation of droplets became possible. The droplet size of control SPI ink was mostly distributed in the range of 20–80 μm. On the contrary, in the presence of surface-active biopolymers, the oil droplets were more closely packed together with the smaller size, which was in agreement with the light scattering results. As visualized from Fig. 10, three fluorescence images were provided for each ink-based emulsion, including oil phase (right column), protein/biosurfactants stained red (middle column), and both oil and protein/biosurfactants stained i.e., overlapping images prepared with exciting Nile Red and Nile Blue A (left column). Regarding the overlap fluorescence images, the oil phase is located in the interior of the droplet, whereas the red color was existent as a shell around the droplets, proposing the formation of an O/W-type emulsion. There was no obvious droplet coalescence in the system, and the size of droplets ranged from 5 to 30 μm. Apparently, the densely packed layer of biosurfactants around the droplets offered the improved stability of the SPI-based ink (Zeng et al., 2017).

The fluorescence images of the EHEC- (Fig. 10a, rows I) and DS inulin- (Fig. 10b, rows II) containing inks showed the droplets were present in the separated and non-flocculated form having a droplet size distribution ranging from 6 to 15 μm, indicating the droplets were homogeneously distributed. This might specify that these inks were surface-active, contained grafted ethyl (hydroxyethyl), dodecenyl succinylate groups, allowing the development of small droplets. For ink-based emulsions formed by OSA (Fig. 10c, rows III) and acetylated starches (Fig. 10d, rows IV), droplet size distribution displayed a shift to larger sizes with somewhat big droplets compared to those formed by EHEC and DS inulin. The interfacial structure reflected the fact that the biopolymeric surfactants adsorbed at the oil/water interface, promoting stable O/W-type emulsions, which enhanced the storage stability against coalescence, flocculation, and Ostwald ripening (Prochaska et al., 2007). Hong, Li, Gu, Wang, and Pang (2017) confirmed the hydrophobically modified starch could form a stable emulsion with more efficiently dispersed oil droplets. Kokubun et al. (2018) also showed that hydrophobically inulin was efficient at decreasing the interfacial tension at the air/water and oil/water interfaces, facilitating the stabilization of O/W-type emulsions. Dai, Sun, Wei, Mao, and Gao (2018) stated that zein/gum Arabic complex colloidal nanoparticles developed a dense and thick interface layer as a shell around the spherical oil droplets, creating a steric barrier in the Pickering emulsion against Ostwald ripening and coalescence.

3.7. Sample selection for the 3D printing process

According to the above discussions, it possibly could be determined that the highly desirable SPI-based inks for the 3D printing process not
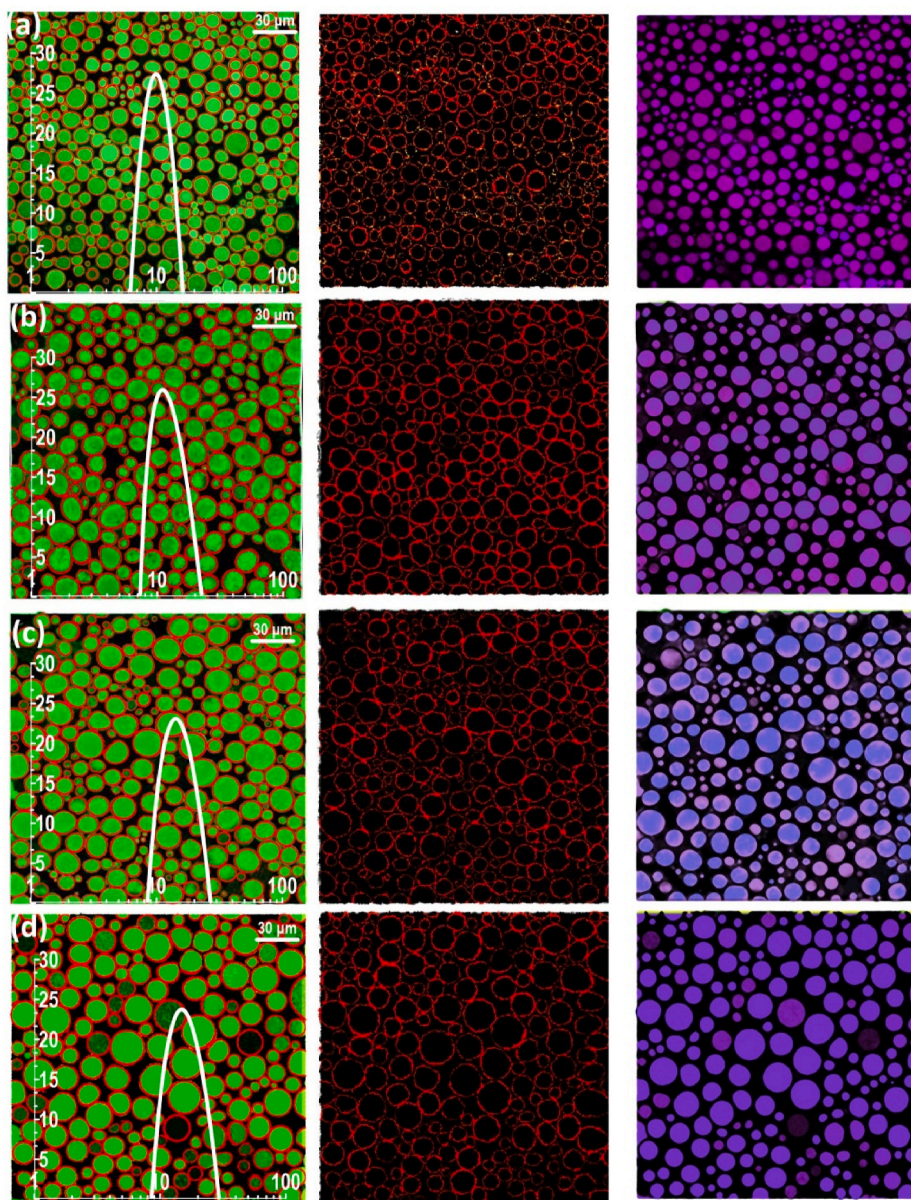
Fig. 10. CLSM images of SPI-based inks stabilized by a): EHEC, (b): DS inulin, (c): OSA starch, and (d): acetylated starch. Oil phase (right column) (for better clarification the green color was changed to purple-blue), protein/biosurfactants stained red (middle column), and overlapping images (left column). (For interpretation of the references to color in this figure legend, the reader is referred to the Web version of this article.)

only possess suitable rheological parameters with enhanced storage emulsion stability against coalescence/flocculation but should also show *pseudoplasticity* and viscoelasticity to be easily extruded out from the nozzle tip in an extrusion-based type printer. Moreover, a thixotropic ink with smaller droplets that are homogeneously distributed in the system might allow reduced-fat ink-based emulsions to improve mechanical stability upon printing. Reportedly, the combination of ink with a monomodal particle size distribution, viscoelastic properties, thixotropic features, and shear-thinning behavior offers an effective way to print 3D objects with a good printing performance (Lee et al., 2019; Shahbazi & Jäger, 2020; Wu et al., 2016). Therefore, a good balance must be made so that the inks show as strong as possible to preserve the printed structure while still could be printable and capable of adhering to previously deposited layers. When the instrumental data for each ink containing surface-active biopolymers were looked at collectively, MAC-60 with the highest viscosity recovery, yield point, G'_{LVR}, and smallest particle size and lowest creep compliance, presented a strong gel-structure. This ink may need more energy for initiating structural

breakdown upon shear force in the 3D printer but can flow easily owing to its thixotropic behavior and *pseudoplasticity*. The MAI-80 shared similarities with MAC-60 in terms of dynamic and static rheological properties. It showed a higher consistency index, G'_{LVR}, with dynamic and recoverable networks, which might also be able to support the deposited layer and maintain the printed shape. The MAO-60 displayed a fairly strong gel structure with improved emulsion stability, albeit having a lower consistency index, yield point, G'_{LVR}, and higher particle size in contrast to MAC-60 and MAI-80. Similarly, MAA-60 showed an improved consistency index, yield point, G'_{LVR}, and emulsion stability with thixotropic feature and shear-thinning behavior, which may be able to provide desired structural stability and high resistance against any shear force in the 3D printer. As noted above, the effects of surface-active biopolymers in the range of 60–80% on the stabilization of SPI-based ink were due to changes in rheological properties and transient behavior of the viscoelastic properties of SPI ink. This could be relatively owing to *(i)*: the existence of intermolecular interactions between functional groups of biosurfactants with

hydrophilic/hydrophobic domains of SPI/oil system, *(ii)*: an increase in the total solids content, *(iii)*: promoting the initiation of separate molecules overlap and inducing a gel-like network, and *(iv)*: developing a densely packed interface layer of biosurfactants around the droplets. In this context, the biosurfactants with lower critical overlap concentration, higher coil-overlap parameter, and greater compact conformation induced more changes in the functional properties of the ink-based emulsion.

4. Conclusions

The reduced-fat soy protein emulsion gels were prepared by total or partial replacement of oil with different biosurfactants to select the optimum ink aimed at potential application in the 3D printing process. Dynamic and steady rheological parameters, particle size distribution, and creep-recovery measurements were considered as a benchmark to select the superior ink formulation for printing application. The inks with higher ratios of surface-active biopolymers presented shear-thinning behavior and an increase in biosurfactants concentration led to an increase in viscosity recovery, yield stress, and elastic modulus. Biosurfactant replacement also moved the crossover point to the higher strains and frequencies due to the development of more structured systems with enhanced connected structures. Biosurfactants with a lower polydispersity index and higher radius of gyration offered an ink with strong *pseudoplasticity*. The formation of a viscoelastic system with higher biosurfactants levels might have benefits for the ability of a 3D printed material to retain its shape over time and achieve good resolution after printing improving the texture and mouthfeel of reduced-fat products. The oil droplets in the emulsion gels stabilized by ethyl (hydroxyethyl) cellulose were the smallest and most uniform followed by modified inulin, while the oil droplets in the emulsion gels with modified starches were relatively large. The rheological properties derived from both dynamic and steady shear flow data, as well as droplet sizes, were fully consistent with the network microstructure, indicating the ink preparation and the testing procedure were satisfactory. Data from thixotropic measurements suggested biosurfactant replacement provided a reversible network structure with the restoration of the initial structures upon breakdown. The results suggested that biosurfactants replacement provided a soy protein-based ink with a monomodal particle size distribution, shear-thinning behavior, thixotropic properties, and viscoelastic properties, gaining a profound understanding of biomaterials printability and extrudability.

Funding

Author statement

Mahdiyar Shahbazi: Conceptualization, Methodology investigation, Collecting data, Validation, Data interpretation, Funding acquisition, Writing – Original draft, Writing – Review & Editing. Henry Jäger: Review & Editing, Validation, Supervision. Rammile Ettelaie: Data interpretation, Writing – Review & Editing. Jianshe Chen: Writing – Review & Editing.

Declaration of competing interest and Compliance with ethics requirements

The authors declare no conflict of interest.

Appendix A. Supplementary data

Supplementary data to this article can be found online at https://doi.org/10.1016/j.foodhyd.2021.106967.

References

Aacc, C. (2000). Approved methods of the American association of cereal chemists. *Methods, 54*, 21.

Asgar, M., Fazilah, A., Huda, N., Bhat, R., & Karim, A. A. (2010). Nonmeat protein alternatives as meat extenders and meat analogs. *Comprehensive Reviews in Food Science and Food Safety, 9*(5), 513–529.

Auty, M. A., Twomey, M. Y. R. A., Guinee, T. P., & Mulvihill, D. M. (2001). Development and application of confocal scanning laser microscopy methods for studying the distribution of fat and protein in selected dairy products. *Journal of Dairy Research, 68*(3), 417–427.

Bai, L., Huan, S., Li, Z., & McClements, D. J. (2017). Comparison of emulsifying properties of food-grade polysaccharides in oil-in-water emulsions: Gum Arabic, beet pectin, and corn fiber gum. *Food Hydrocolloids, 66*, 144–153.

Bohrer, B. M. (2019). An investigation of the formulation and nutritional composition of modern meat analogue products. *Food Science and Human Wellness, 8*(4), 320–329.

Chen, J., Mu, T., Goffin, D., Blecker, C., Richard, G., Richel, A., et al. (2019). Application of soy protein isolate and hydrocolloids based mixtures as promising food material in 3D food printing. *Journal of Food Engineering, 261*, 76–86.

Dai, L., Sun, C., Wei, Y., Mao, L., & Gao, Y. (2018). Characterization of Pickering emulsion gels stabilized by zein/gum Arabic complex colloidal nanoparticles. *Food Hydrocolloids, 74*, 239–248.

Dickinson, E. (2012). Emulsion gels: The structuring of soft solids with protein-stabilized oil droplets. *Food Hydrocolloids, 28*(1), 224–241.

Dickinson, E., & Galazka, V. B. (1991). Emulsion stabilization by ionic and covalent complexes of β-lactoglobulin with polysaccharides. *Food Hydrocolloids, 5*(3), 281–296.

Ding, Y., Chen, L., Shi, Y., Akhtar, M., Chen, J., & Ettelaie, R. (2021). Emulsifying and emulsion stabilizing properties of soy protein hydrolysates, covalently bonded to polysaccharides: The impact of enzyme choice and the degree of hydrolysis. *Food Hydrocolloids, 113*, 106519.

Doi, M., Edwards, S. F., & Edwards, S. F. (1988). *The theory of polymer dynamics, 73*. oxford university press.

Elomaa, M., Asplund, T., Soininen, P., Laatikainen, R., Peltonen, S., Hyvärinen, S., et al. (2004). Determination of the degree of substitution of acetylated starch by hydrolysis, 1H NMR and TGA/IR. *Carbohydrate Polymers, 57*(3), 261–267.

Flores, M., Giner, E., Fiszman, S. M., Salvador, A., & Flores, J. (2007). Effect of a new emulsifier containing sodium stearoyl-2-lactylate and carrageenan on the functionality of meat emulsion systems. *Meat Science, 76*(1), 9–18.

Genccelep, H., Saricaoglu, F. T., Anil, M., Agar, B., & Turhan, S. (2015). The effect of starch modification and concentration on steady-state and dynamic rheology of meat emulsions. *Food Hydrocolloids, 48*, 135–148.

Godoi, F. C., Prakash, S., & Bhandari, B. R. (2016). 3d printing technologies applied for food design: Status and prospects. *Journal of Food Engineering, 179*, 44–54.

Hong, Y., Li, Z., Gu, Z., Wang, Y., & Pang, Y. (2017). Structure and emulsification properties of octenyl succinic anhydride starch using acid-hydrolyzed method. *Starch Staerke, 69*(1–2), 1600039.

Huggins, M. L. (1942). The viscosity of dilute solutions of long-chain molecules. IV. Dependence on concentration. *Journal of the American Chemical Society, 64*(11), 2716–2718.

Hyun, K., Kim, S. H., Ahn, K. H., & Lee, S. J. (2002). Large amplitude oscillatory shear as a way to classify the complex fluids. *Journal of Non-newtonian Fluid Mechanics, 107*(1–3), 51–65.

Hyun, K., Wilhelm, M., Klein, C. O., Cho, K. S., Nam, J. G., Ahn, K. H., et al. (2011). A review of nonlinear oscillatory shear tests: Analysis and application of large amplitude oscillatory shear (Laos). *Progress in Polymer Science, 36*(12), 1697–1753.

Karlberg, M., Thuresson, K., & Lindman, B. (2005). Hydrophobically modified ethyl (hydroxyethyl) cellulose as stabilizer and emulsifying agent in macroemulsions. *Colloids and Surfaces A: Physicochemical and Engineering Aspects, 262*(1–3), 158–167.

Kiumarsi, M., Majchrzak, D., Jäger, H., Song, J., Lieleg, O., & Shahbazi, M. (2021). Comparative study of instrumental properties and sensory profiling of low-calorie chocolate containing hydrophobically modified inulin. Part II: Proton mobility, topological, tribological and dynamic sensory properties. *Food Hydrocolloids, 110*, 106144.

Kiumarsi, M., Majchrzak, D., Yeganehzad, S., Jäger, H., & Shahbazi, M. (2020). Comparative study of instrumental properties and sensory profiling of low-calorie chocolate containing hydrophobically modified inulin. Part 1: Rheological, thermal, structural and external preference mapping. *Food Hydrocolloids, 104*, 105698.

Kiumarsi, M., Shahbazi, M., Yeganehzad, S., Majchrzak, D., Lieleg, O., & Winkeljann, B. (2019). Relation between structural, mechanical and sensory properties of gluten-free bread as affected by modified dietary fibers. *Food Chemistry, 277*, 664–673.

Kokubun, S., Ratcliffe, I., & Williams, P. A. (2015). The emulsification properties of octenyl-and dodecenyl-succinylated inulins. *Food Hydrocolloids, 50*, 145–149.

Kokubun, S., Ratcliffe, I., & Williams, P. A. (2018). The interfacial, emulsification and encapsulation properties of hydrophobically modified inulin. *Carbohydrate Polymers, 194*, 18–23.

Kraemer, E. O. (1938). Molecular weights of celluloses and cellulose derivates. *Industrial and Engineering Chemistry, 30*(10), 1200–1203.

Lee, J. H., Won, D. J., Kim, H. W., & Park, H. J. (2019). Effect of particle size on 3D printing performance of the food-ink system with cellular food materials. *Journal of Food Engineering, 256*, 1–8.

Liu, F., & Tang, C. H. (2011). Cold, gel-like whey protein emulsions by microfluidisation emulsification: Rheological properties and microstructures. *Food Chemistry, 127*(4), 1641–1647.

Malav, O. P., Talukder, S., Gokulakrishnan, P., & Chand, S. (2015). Meat analog: A review. *Critical Reviews in Food Science and Nutrition, 55*(9), 1241–1245.

Malone, M. E., & Appelqvist, I. A. (2003). Gelled emulsion particles for the controlled release of lipophilic volatiles during eating. *Journal of Controlled Release, 90*(2), 227–241.

Menard, K. P., Menard, N., & Dynamic mechanical analysis. (2006). Encyclopedia of analytical Chemistry: Applications. *Theory and Instrumentation*, 1–25.

Morris, E. R., Cutler, A. N., Ross-Murphy, S. B., Rees, D. A., & Price, J. (1981). Concentration and shear rate dependence of viscosity in random coil polysaccharide solutions. *Carbohydrate Polymers, 1*(1), 5–21.

Morrison, W. R., & Laignelet, B. (1983). An improved colorimetric procedure for determining apparent and total amylose in cereal and other starches. *Journal of Cereal Science, 1*(1), 9–20.

Prochaska, K., Kędziora, P., Le Thanh, J., & Lewandowicz, G. (2007). Surface activity of commercial food grade modified starches. *Colloids and Surfaces B: Biointerfaces, 60* (2), 187–194.

Shahbazi, M., & Jäger, H. (2020). Current status in the utilization of biobased polymers for 3D printing process: A systematic review of the materials, processes, and challenges. *ACS Applied Bio Materials, 4*(1), 325–369.

Shahbazi, M., Jäger, H., Ahmadi, S. J., & Lacroix, M. (2020). *Electron beam crosslinking of alginate/nanoclay ink to improve functional properties of 3D printed hydrogel for removing heavy metal ions* (p. 116211). Carbohydrate Polymers.

Shahbazi, M., Jäger, H., & Ettelaie, R. (2021a). Application of Pickering emulsion and 3D printing for personalized nutrition. Part I: Development of reduced-fat printable cheese analogue ink. *Colloids and Surfaces A: Physicochemical and Engineering Aspects*, 126641.

Shahbazi, M., Jäger, H., & Ettelaie, R. (2021b). Application of Pickering emulsion and 3D printing for personalized nutrition. Part II: Functional properties of reduced-fat 3D printed cheese analogues. *Colloids and Surfaces A: Physicochemical and Engineering Aspects*, 126760.

Shahbazi, M., Rajabzadeh, G., Rafe, A., Ettelaie, R., & Ahmadi, S. J. (2017). Physico-mechanical and structural characteristics of blend film of poly (vinyl alcohol) with biodegradable polymers as affected by disorder-to-order conformational transition. *Food Hydrocolloids, 71*, 259–269.

Smidsrød, O., & Haug, A. (1971). Estimation of the relative stiffness of the molecular chain in polyelectrolytes from measurements of viscosity at different ionic strengths. *Biopolymers: Original Research on Biomolecules, 10*(7), 1213–1227.

Sun, C., & Gunasekaran, S. (2009). Effects of protein concentration and oil-phase volume fraction on the stability and rheology of menhaden oil-in-water emulsions stabilized by whey protein isolate with xanthan gum. *Food Hydrocolloids, 23*(1), 165–174.

Tadros, T. (2009). Polymeric surfactants in disperse systems. *Advances in Colloid and Interface Science, 147*, 281–299.

Tadros, T. F., Vandamme, A., Levecke, B., Booten, K., & Stevens, C. V. (2004). Stabilization of emulsions using polymeric surfactants based on inulin. *Advances in Colloid and Interface Science, 108*, 207–226.

Tang, C. H., & Liu, F. (2013). Cold, gel-like soy protein emulsions by microfluidization: Emulsion characteristics, rheological and microstructural properties, and gelling mechanism. *Food Hydrocolloids, 30*(1), 61–72.

Thanasukarn, P., Pongsawatmanit, R., & McClements, D. J. (2004). Influence of emulsifier type on freeze-thaw stability of hydrogenated palm oil-in-water emulsions. *Food Hydrocolloids, 18*(6), 1033–1043.

Wang, Y., Li, D., Wang, L. J., & Adhikari, B. (2011). The effect of addition of flaxseed gum on the emulsion properties of soybean protein isolate (SPI). *Journal of Food Engineering, 104*(1), 56–62.

Wang, S., Yang, J., Shao, G., Qu, D., Zhao, H., Yang, L., & Zhu, D. (2020). Soy protein isolated-soy hull polysaccharides stabilized O/W emulsion: Effect of polysaccharides concentration on the storage stability and interfacial rheological properties. *Food Hydrocolloids, 101*, 105490.

Watanabe, A., Daly, C. C., & Devine, C. E. (1996). The effects of the ultimate pH of meat on tenderness changes during ageing. *Meat Science, 42*(1), 67–78.

Wu, H., Cheng, Y., Liu, W., He, R., Zhou, M., Wu, S., & Chen, Y. (2016). Effect of the particle size and the debinding process on the density of alumina ceramics fabricated by 3D printing based on stereolithography. *Ceramics International, 42*(15), 17290–17294.

Yang, L., & Zhang, L. M. (2009). Chemical structural and chain conformational characterization of some bioactive polysaccharides isolated from natural sources. *Carbohydrate Polymers, 76*(3), 349–361.

Zeng, T., Wu, Z. L., Zhu, J. Y., Yin, S. W., Tang, C. H., Wu, L. Y., et al. (2017). Development of antioxidant Pickering high internal phase emulsions (HIPEs) stabilized by protein/polysaccharide hybrid particles as potential alternative for PHOs. *Food Chemistry, 231*, 122–130.

Zhang, J. Y., Pandya, J. K., McClements, D. J., Lu, J., & Kinchla, A. J. (2021). Advancements in 3D food printing: A comprehensive overview of properties and opportunities. *Critical Reviews in Food Science and Nutrition*, 1–18.